Author version: *J. Asian Earth Sci., vol.70-71; 2013; 125-141*

Geochemical variability of MORBs along slow to intermediate spreading Carlsberg-Central Indian Ridge, Indian Ocean

D. Ray[1*], S. Misra[2] and R. Banerjee[3]

[1]PLANEX, Physical Research Laboratory, Ahmedabad 380 009, India

[2]School of Geological Sciences, University of KwaZulu-Natal, Durban- 4000, South Africa

[3]CSIR-National Institute of Oceanography, Goa-403004, India

[*]Corresponding author's e-mail: dwijeshray@gmail.com, dwijesh@prl.res.in

Abstract

We present new major and ICP-MS trace element data of the Carlsberg Ridge MORBs from two different locations (i.e., 3°35′N/64°05′E and 3°41′N/64°09′E) and reassess the intra-ridge geochemical variations of Carlsberg Ridge- Central Indian Ridge MORBs in the present work. Geochemically, the trace element contents of the Carlsberg Ridge MORBs are similar to the Rodriguez Triple Junction MORBs [e.g., LIL and REE spidergrams and $(La/Sm)_N$ ratio etc.] and both are closely resembling to the average N-MORB in composition. The MORBs from the northern- and southern Central Indian Ridge, however, significantly vary in composition between average N- and E-MORBs. The Carlsberg Ridge- Central Indian Ridge MORBs, in general, show much less fractionation in FeO_t in MgO-CaO-FeO_t diagram compared to those of the Mid Atlantic- and East Pacific Rise MORBs. Further, the depleted LREE and nearly flat HREE patterns of the Carlsberg Ridge- Central Indian Ridge MORBs, along with their least variability of compatible trace element (Ni, Cr, Sr) contents against increasing incompatible trace element (Y, Zr) contents in the log-log plots and their increasing incompatible trace element ratios in the process identification plots favor partial melting dominated process for their petrogenetic evolution. Our review on isotope data (Sr, Nd, Pb) shows that the Carlsberg Ridge-Central Indian Ridge MORBs were derived from a depleted mantle source that was variously contaminated by continental crust perhaps during the third stage of Gondwana break up between 155-135 Ma or later due to the strike slip movement along a mega fracture, a member of the Davie Transform Faults in the Somali Basin, that broke the Gondwanaland into the East and West Gondwanas and during subsequent movement of these two blocks away from each other. The $^{208}Pb/^{204}Pb$ versus $^{206}Pb/^{204}Pb$ plot of above mentioned MORBs suggests that the depleted mantle source of the Rodriguez Triple Junction MORBs was contaminated by ~21% lower continental crust, whereas the mantle source of the Central Indian Ridge MORBs was contaminated by upper continental crust, which are ~19% for the Carlsberg Ridge and Northern Central Indian Ridge MORBs and ~32% for the Southern Central Indian Ridge MORBs. The contaminated mantle sources were compositionally similar to the Al-depleted Komatiite basalt in composition and significantly enriched in Rb, Ba, La and Ce over the depleted mantle.

Key words: Carlsberg-Central Indian Ridge (CR-CIR) MORBs, Partial melting, Mantle contamination, Continental crust, Gondwana breakup, Komatiitic source.

1. Introduction

The Indian Ocean Ridge System (IORS), a ~9500 km-long chain of active submarine volcanoes, is one of the most prominent and characteristic features in the Indian Ocean (Fig. 1a). This inverted 'Y' -shaped looking ridge system has an axial height of ~100-800 m above the sea floor and a width of 1-23 km (Parson et al., 1993; Drolia et al., 2003 and Kamesh Raju et al., 2008), which is transected and displaced by numerous NNE-SSW trending transform faults (TFs) among which Owen, Mahabiss, Sealark, Vityaz, Vema, Argo, Marie Celeste, Egeria and Gemino TFs are more prominent (Iyer and Ray, 2003).

The IORS has been subdivided into six ridge segments from north to south on the basis of spreading rates, i. e., the Carlsberg Ridge (CR), Northern Central Indian Ridge (NCIR) and Southern Central Indian Ridge (SCIR); which all together are known as the Central Indian Ridge (CIR); and the Rodriguez Triple Junction (RTJ), South East Indian Ridge (SEIR) and South West Indian Ridge (SWIR) (after Schlich, 1982) (Fig. 1a). The ~4200 km-long Carlsberg-Northern Central Indian Ridge (CR-NCIR) is one of the youngest, complex and perhaps the least studied ocean ridge system in comparison to the SCIR, SEIR and SWIR (Christie et al., 1998; Mahoney et al., 2002; Meyzen et al., 2003; Murton et al., 2005; Nauret et al., 2006; Ray et al., 2007; Ray et al., 2011). The spreading rates along the CR-CIR gradually increase from the north to south along its length: the CR has the lowest half spreading rate of ~11-16 mm/yr (Chaubey et al., 1993; Ramana et al., 1993; Kamesh Raju et al., 2008); the NCIR corresponds to slow to intermediate half spreading rate of ~18-21 mm/yr (Drolia and DeMets, 2005), the SCIR spreads at intermediate half spreading rate of ~23 mm/yr (Royer et al., 1997), while half spreading rate of ~27 mm/yr is highest at the RTJ (Munschy and Schlich, 1989).

The Mid-Ocean Ridge Basalts (MORBs) from the IORS, in general, differ both in their trace element as well as isotopic contents compared to those from the East Pacific Rise (EPR) and Mid-Atlantic Ridge (MAR). The K, Rb and Sr contents of MORBs from the IORS are in general, higher than those of the MAR and EPR MORBs (Subbarao and Hedge, 1973). Further, the radiogenic isotopic studies show that the IORS MORBs have consistently higher $^{208}Pb/^{204}Pb$ ratios compared to those of the Pacific MORBs, many of the IORS MORBs even have lower ε_{Nd} and higher $^{87}Sr/^{86}Sr$ ratios than those of the EPR MORBs (Hofmann, 2003; also Price et al., 1986; Mahoney et al., 1989). These distinct isotopic characteristics are thought to be the result of a large-scale mantle contamination, either by ancient recycled sediments or delaminated subcontinental lithosphere (Rehkämper and Hofmann, 1997).

Although a comprehensive isotopic and geochemical comparison between the Atlantic, Pacific and IORS MORBs exists (Hofmann, 2003; Arevalo and McDonough, 2010), any intra-ridge geochemical and isotopic comparison among the segments of IORS, however, are only partially known, which is due to limited available geochemical data especially from the CR and NCIR sectors of the IORS (Fig. 1). Till date, most of the petrochemical investigations have been centered in and along the SCIR or RTJ mainly to explore the possible relationship between the Reunion plume and evolving triple junction present in this area (Price et al., 1986; Humler and Whitechurch, 1988, Rehkämper and Hofmann, 1997, Murton et al., 2005 and Nauret et al., 2007). Based on limited geochemical data, Hekinian (1968) and Subbarao et al. (1977, 1979) concluded that the CR MORBs are compositionally distinct from IORS MORBs by having typical N-MORB characters (i.e., depleted in incompatible trace elements), which is the general characteristic for slow spreading ridge (e.g., MAR) MORBs. However, detailed geochemical data of MORBs from several locations on the CR are still inadequate in order to understand its petrogenetic evolutionary process.

The aims of our present study are, therefore, (1) to present newly generated geochemical data of CR MORBs from two different locations in the CR (Fig. 1b), and (2) to make a comparative geochemical study of the MORBs from different sectors of IORS only up to the RTJ to evaluate the petrogenetic evolutionary processes. Besides our present data on the CR MORBs, the geochemical and isotopic data on the NCIR, SCIR and RTJ, and additional data on the CR have been collated from literature (Price et al., 1986; Banerjee and Iyer, 2003; Herzig and Pluger, 1988; Humler and Whitechurch, 1988; Pluger et al., 1988; Mahoney et al., 1989; Natland, 1991; Rehkämper and Hofmann, 1997; Murton et al., 2005; Nauret et al., 2006; Ray et al., 2007 and PetDB, online at http://petdb.ldeo.columbia.edu/petdb/) for the present comparison.

Our attempt, however, excludes any discussion on the intra-ridge geochemical variability that exists within the SWIR near RTJ (e.g. Meyzen et al., 2003). Even though the bathymetric studies revealed the existence of several second order discontinuities and non-transform discontinuities within the SCIR (Briais, 1995); the magnetic and topographic variations are further amplified intra-segmental complexities among different ridge-segments of the CIR, SEIR and SWIR (Honsho et al., 1996). However the present study exclude the possible roles of these tectonic features on the petrochemistry of the IORS MORBs.

2. Morphology of the Carlsberg Ridge

The Carlsberg Ridge defines the divergent plate boundary between the Indian and Somalian plates (Fig. 1a), which has opened during the late Paleocene (~55 Ma) when the Seychelles bank

separated out from the Indian plate (McKenzie and Sclater, 1971). The Owen fracture zone in the northwest offsets the CR axis by about 350 km. Towards the southeast, the trend of the CR rotates from the NW–SE to nearly N–S as it meets the NCIR near the equator. Although a few discrete regional geophysical studies were available on the Indian Ocean (McKenzie and Sclater, 1971; Schlich, 1982; Royer and Sandwell, 1989), the multibeam swath bathymetry maps along a few segments of the CR (at 62°20'E and 66°20'E) were first reported in Kamesh Raju et al. (1998, 2008) and Mudholkar et al. (2002). The CR is characterized by rugged topography, steep inner valley walls and wide rift valley floor (~13-26 km), with an axial volcanic ridge ranging in heights between ~200-800 m and length of ~5-23 km, which are similar to the slow spreading ridge segment of the northern MAR. The CR has a NW–SE trend, after then the gradual bend in the ridge axis is accommodated by non-transform discontinuities and along-axis bathymetric deeps.

3. Sampling and analytical technique

During the maiden cruise of the ORV Sagar Kanya in 1983, a small area of CR was sampled (small boxes in inset figure 1). Two dredge operations (dr 1~ 3°35′N, 64°05′E and dr 2 ~3°41′N, 64°09′E at an average water depth of 3750 m) were carried out along the rift valley based on the geological world atlas of UNESCO (1976). The dredges were operated mainly based on single-beam bathymetry. Recently, Kamesh Raju et al. (2008) has published the multibeam bathymetry map of the study area. On the basis of those maps, the CR sample locations fall close to the ridge axis (as shown in white lines in figure 1,inset) well within the magnetic chron 2 (Fig.1).

The fresh rock chips from each sample (total 18 in number) were powdered using an agate ball mill at the National Institute of Oceanography, Goa, India, for whole-rock chemical analyses. The major oxide analyses of the selected samples of the CR MORBs (Table 1) were carried out at the Indian Institute of Technology, Kharagpur, India, by XRF (model Philips PW 2404) technique on fused pellets. The accuracy and precision of analyses observed for the International rock standards MO-12 [Andesite-Basalt; IGEM] and W2 [Diabase; USGS] were better than 5% and ±2% respectively. In total 18 CR MORB samples (12 from location dr 01 and 6 from location dr 02) were analyzed for trace elements (Table 1) by inductively coupled plasma-mass spectrometry (ICP-MS, model ELAN DRC II, Perkin Elmer Sciex Instruments, USA) at the National Geophysical Research Institute, Hyderabad, India, following the procedure described in Balaram et al. (1999) and Ray et al. (2007). Two runs on the International rock standard JB-2 (Japanese basalts) was carried out in the initial and final stages of the analyses. The accuracies of analyses for all the trace elements were better than ±5%. All the elements with atomic number between Sc and Ba showed analytical precisions better than 4.5%, except those between La and U, which had precision better than 7.5%.

4. Petrography and mineral chemistry of CR-CIR MORBs

The dredge recoveries mostly include pillow lavas with thin glassy veneer (1-3 mm thickness) at the outer part of each pillow. Glasses of the pillow-rims characteristically display vitreous to sub-vitreous luster with conchoidal fractures. The CR basalts, under microscope, are mostly fine grained, porphyritic basalts where tiny phenocrysts of plagioclase and rare olivine crystals are embedded in a dark coloured glassy matrix (Fig 2a). The interstitial spaces of plagioclase microlites in the groundmass are occupied by glassy materials resulting an interstitial texture. Occasionally, the plagioclase and olivine phenocrysts together constitute local clusters, which can be described as the glomeroporphyritic structure (Fig 2b). Both normal and reverse compositional zoning along with twining are present in the prismatic plagioclase phenocrysts (Fig. 2c). The euhedral prismatic plagioclase phenocrysts often display corroded "skeletal" structure (Fig. 2d) indicating possible reaction between the early formed plagioclase and late magma. The plagioclase phenocrysts often show irregular outline, hosting a few glassy melt inclusions, locally devitrified (Fig. 2e). The plagioclases particularly from the inner part of the pillows are skeletal in shape while olivines show doubly swallow-tail structure (Fig. 2f). The clinopyroxene (mainly diopsidic) phenocryst is rarely present in a few samples. The mineralogical features of the IORS MORBs are either fine grained glassy basalts or Moderately Phyric Plagioclase Olivine Basalts (MPPOB, after Hekinian, 1982; Table 2), where anhedral to euhedral, skeletal grains of olivine rarely occur as microphenocrysts. The textural and mineral assemblages of CR basalt observed in the present study suggest they are similar to Moderately Phyric Plagioclase Basalt (MPPB, after Hekinian, 1982).

In CR MORBs, the plagioclase phenocrysts and microphenocrysts are relatively calcic in composition (An_{82-87}, in average An_{85}) with low K_2O (0.02 to 0.29 wt%; average 0.06 wt%) compared to the plagioclase laths in the groundmass (An_{67-79}, in average An_{74}), which have K_2O from 0.03-0.45 wt% (average 0.10 wt%). The olivine varies in composition between Fo_{83-91} (average Fo_{88}) with NiO contents up to 0.36 wt% (Iyer and Banerjee, 1993) (Fig. 3). The compositional zoning in olivine is rare.

The CR MORBs are petrographically similar to the NCIR basalts, which have an affinity towards the MPPB (Hekinian, 1982). However, the NCIR MORBs contain more olivine (up to 1.69 vol%) and rare clinopyroxene phenocrysts (Ray et al., 2009). The plagioclases occur as phenocrysts (An_{63-85}) and as laths in groundmass (An_{52-72}) in the NCIR MORBs, however, are more evolved compared to those in the CR MORBs (Table 2). The phenocrystic olivine compositions in the NCIR MORBs vary from Fo_{81-86} and are very similar in composition to those in the CR MORBs. The clinopyroxenes in the NCIR MORBs are mainly diopsidic (see Fig S1 in supplementary materials)

($Wo_{42-51}En_{21-38}Fs_{14-26}$) (Ray et al., 2009) and are evolved at relatively low temperature (<800^{o}C) (Ray et al., 2011).

The CR and NCIR MORBs differ in petrography to those observed in the SCIR and RTJ MORBs. The SCIR basalts are MPPOB type under microscope (Sauter et al., 1996). The plagioclases in the SCIR MORBs show a moderate compositional variation from An_{76} in groundmass laths up to An_{90} in phenocryst and the olivine shows minimum compositional variation (Fo_{89-92}). The RTJ basalts are generally plagioclase and olivine phyric (MPPOB) (Price et al., 1986). Olivine is present as phenocryst with restricted compositional range ($Fo_{84.7-89.6}$). Plagioclase is equally abundant as megacryst (An_{81-93}) and as laths in the groundmass (An_{67-72}). Melt inclusions are present both within the phenocrysts of plagioclase and olivine.

The opaque mineralogy of the CR-CIR MORBs is only partially known. The opaques in the CR basalts mainly include disseminated pyrrhotite, pyrite, chalcopyrite and magnetite grains of magmatic origin (Banerjee and Iyer, 1993). The Ni content of the sulphide grains are low (i.e. 0.14-1.82 wt%; average ~0.71 wt%, n=15 points, unpublished data of R. Banerjee), and the incorporation of Ni might have taken place from the basaltic parent magma (Peach et al., 1990). Our petrographic observation on the CR MORBs also shows the absence of any secondary vein associated with these sulphide mineral assemblages, which further consolidates the concept of their magmatic origin rather than by any hydrothermal process. The opaques in the NCIR MORBs are mainly titanomagnetite that occur within the groundmass or as inclusions within the plagioclase (Ray et al., 2009). No chromian spinel is observed under microscope either in the NCIR or CR MORBs. Information on opaque mineralogy and mineral chemistry in the SCIR and RTJ MORBs, however, is inadequate in literature.

5. Whole-rock geochemistry of CR-CIR MORBs

5.1.Major element chemistry

The terrestrial and planetary basaltic rocks could be examined in $CaO+Na_2O+K_2O+MgO$ (CNKM)-FeO^T-Al_2O_3 plot (after Nesbitt and Wilson, 1992) to evaluate the effect of surface weathering (e.g. Newsom et al., 2010). This diagram is also used in the present study to examine the effect of any possible sea-water alteration on the CR-CIR MORBs (Fig. 4). Our present data on the CR and literature data on the NCIR, SCIR and RTJ MORBs show a point concentration of plots between the CNKM apex and the feldspar line. The clustering of all data and their high relative proportions of CNKM (~40-50 wt%) suggest that the MORB samples under examination collected

from the different sectors of ~4200 km long CR-CIR ridge do not have any major effect of variable sea-water interaction.

The major oxide compositions of different ridge domains along the IORS are compared in Table 3. The SiO_2 of the CR-CIR MORBs are close to that of the average primitive-MORB i.e. ~49.8 wt% (Presnall and Hoover, 1987) and show very restricted range of variation (~48-53 wt%), except the NCIR basalts, that shows marginally wide variation (46-52 wt%). These MORBs from the four sectors of CR-CIR have similar average Magnesium number (Mg# ~0.61), CaO/Al_2O_3 (~0.73), K_2O/Na_2O (~0.05) and Na_2O+K_2O (~2.7 wt%). The CR-CIR MORBs are compared with the type-I, II and III IORS basalts in TiO_2 versus Na_2O diagram (after Natland, 1991) (Fig. 5a), where oceanic basalts were classified on the basis of their Na_2O and TiO_2 contents, viz. low TiO_2-Na_2O type I basalt, and high TiO_2-Na_2O type III basalt and an intermediate TiO_2-Na_2O type II basalt. While the CR basalts show wide variation between type I and III IORS basalts, the RTJ MORBs are mostly close to type II IORS basalt; and the SCIR and NCIR basalts are mostly varying between type I and II, and type II and III IORS basalts respectively.

Further important variations of CR-CIR MORBs are examined in SiO_2 versus (Na_2O+K_2O) plot (Fig. 5b). The majority of samples are plotted within an elliptical field with limited variation in total alkalies between ~ 2 and 3.5 wt% and significant overlap in composition. This plot does not show any specific trend of variation of total alkalies with increasing SiO_2. The FeO^T/ MgO ratios in most of the CR-CIR MORBs are close to ~1 (average=1.17, standard deviation=0.23, n=141) and show no variation with increasing SiO_2 (Fig. 5c).

The relative bulk compositional variations among the Mid Atlantic Ridge (MAR), East Pacific Rise (EPR) and CR-CIR MORBs are compared in MgO-CaO-FeO^T plot (Fig. 5d, data for MAR and EPR MORBs from www.geokem.com/ORB-Oceanic-summary.html). The EPR and MAR MORBs show overlapping composition with distinct trend of FeO_t enrichment. The CR-CIR MORBs are plotted well within this overlapping field but do not show any FeO^T enrichment.

5.2. Trace element chemistry

The primitive mantle normalized (after Sun and McDonough, 1989) incompatible trace element multivariate plots (spider diagram) of MORBs from all the four sectors of the CR-CIR are shown in figure 6. The incompatible trace elements are plotted in this diagram from the left to right along the abscissa in the order of increasing compatibility (cf. Rollinson, 1993). The CR MORBs are, in general, mostly similar to the average N-MORBs, although LIL elements (e.g. Rb and K) show evolved chemistry and compositionally approach to those of the E-MORBs (Fig. 6a). The

incompatible trace element chemistry of the CR MORBs is incidentally similar to that of the RTJ MORBs (Fig. 6b). Enrichments of Rb and K in many samples of the RTJ MORBs are their typical characteristics. The primary mantle normalized incompatible trace element plots of the NCIR and SCIR MORBs are, however, different and show continuous variation for Ba, Rb, K, Nb, La and Ce between the average N- and E-MORBs (Fig. 6c, d).

The chondrite normalized (after McDonough and Sun, 1995) REE plots of the CR-CIR MORBs are shown in figure 7. The REE pattern of the CR basalts is typically LREE depleted (La/Sm_N 0.61-0.71), otherwise it is flat (Ce/Yb_N 0.76-0.97) and similar to the average N-MORB (Fig. 7a). The RTJ MORBs are also LREE depleted (La/Sm_N 0.54-1.07), otherwise mostly flat (Ce/Yb_N 0.75-1.0) and similar to the N-MORB, although variation in actual abundances in LREE between the average N- and E-MORBs is present and few samples show LREE enrichment (Ce/Yb_N ~1.8) (Fig. 7b). The NCIR basalts also show LREE depleted (La/Sm_N 0.46-1.15), and more or less flat REE (Ce/Yb_N 0.67-1.37) pattern similar to the average N-MORBs, although the LREE abundance in these MORBs varies between those of the average N- and E-MORBs, these basalts are relatively enriched in middle and heavy REEs (Fig. 7c). The REE pattern of the SCIR MORBs, however, is different; it shows both LREE depleted and enriched varieties (La/Sm_N ~0.53-1.73) similar to the average N- and E-MORBs respectively, otherwise it has mostly flat REE (Ce/Yb_N ~0.65-1.0) (Fig. 7d).

The trace element ratios of similar incompatible pairs are found to be more useful in identifying source differences among oceanic basalts because they are least affected during partial melting or fractional crystallization (cf. Hofmann, 2003). It is known that the most of the Ocean Island Basalts (OIB) are much enriched in incompatible trace elements and have low Al, Yb and Sc than most of the MORBs (Hofmann, 2003, sec. 2.03.5.2). Therefore, to identify the possible contribution of the OIB mantle source, the CR-CIR MORBs are examined in Mg# versus $(La/Sm)_N$ (cf. Schilling et al., 1983), $(La/Yb)_N$ versus $(Nb/Yb)_N$ and $(Ba/Yb)_N$ plots (Fig.8). In Mg# versus $(La/Sm)_N$ plot, the CR and most of the RTJ MORBs have $(La/Sm)_N$ values close to ~0.6 and these data do not show any variation with decreasing Mg#; three of the RTJ MORBs have $(La/Sm)_N$ close to ~1.00 (Fig. 8a). Therefore, $(La/Sm)_N$ ratios suggest a depleted mantle source for the CR and RTJ MORBs. The NCIR and SCIR MORBs have $(La/Sm)_N$, mostly between ~0.5 and 1.0 but some of the samples have values $\geq$ 1.00, indicating possible involvement of enriched source in their genesis. This finding is also examined in $(La/Yb)_N$ versus $(Nb/Yb)_N$ and $(Ba/Yb)_N$ plot (Figs. 8b, c). Both these plots suggest involvement of the E-mantle or more evolved sources like the OIB or upper continental crust (not shown in the diagram) in the genesis of the NCIR and SCIR MORBs.

Therefore, the CR-CIR MORBs can be classified into two following principal groups on the basis of their incompatible trace element and REE contents, viz.: (a) The CR and RTJ basalts, which are close to N-MORBs in composition, and (b) the NCIR and SCIR basalts showing wide compositional variations mostly between the N- and E-MORBs.

Condie (2003) suggested that Nb/Th, Zr/Nb, Zr/Y and Nb/Y incompatible trace element ratios can be used to characterize some of the isotopic mantle domains for oceanic basalts. The Zr/Y versus Nb/Y space can be efficiently used to discriminate plume- and non-plume sources for the oceanic basalts. As the plume hypothesis is still debatable (e.g. Hamilton, 2011, and references therein), the diagram can safely be used to discriminate the shallow versus deep mantle sources for the oceanic basalts. In the Zr/Y and Nb/Y plot (Fig. 8d), the CR, RTJ and majority of the NCIR basalts form a cluster in the shallow mantle source field of the diagram within the field of N-MORBs (not shown in the diagram) close to the depleted mantle. The SCIR basalts, however, show a different type of distribution. Nearly half of the data are plotted within the N-MORB field together with the CR, RTJ and NCIR basalts; the rest of the SCIR basalts along with a few NCIR MORBs are plotted in the field of oceanic plateau basalt close to the primitive mantle within the domain of the deep mantle source.

5.3. Igneous process of formation

One of the main objectives in our present study is to evaluate the possible igneous process(es) responsible for the evolution of the CR-CIR MORBs and their co-genetic relationship using known geochemical variation diagrams. The clustering of all data at one point and absence of any iron enrichment trend in the CaO-MgO-FeO_t diagram (Fig. 5d), along with absence of any linear increasing trend for alkalies (Na_2O+K_2O) and FeO_t/MgO with increasing SiO_2 (Fig. 5b, c), perhaps rule out the possibility of any bulk fractionation of the magma in the evolution of the CR-CIR MORBs. These geochemical observations altogether suggest against any major fractional crystallization of the parent magma during the evolution of the CR-CIR MORBs. As the possibility of bulk crystal fractionation is an important issue in evaluating the petrogenesis of the CR-CIR MORBs, more sensitive geochemical variation diagrams are used to evaluate the process of formation of these basalts.

The phenocryst population in the CR-CIR basalts include mostly plagioclase and olivine, while the NCIR basalts include clinopyroxene as an additional phenocryst population. Among these three silicate mineral phases, clinopyroxene withdraws most of HREE during its crystallization from basaltic magma, while olivine withdraws HREE to a much lesser extent (Rollinson, 1993; White,

1991; cf. Donnelly et al., 2004). Relatively depleted LREE (La/Sm_N ~0.78) and flat HREE (Gd/Yb_N ~1-1.43) of the CR-CIR MORBs (Fig. 7), therefore, do not suggest any major fractionation of clinopyroxene from the CR-CIR in their parent magma. Absence of any negative Eu anomaly (Fig. 7) also excludes the possibility of any early withdrawal of plagioclase from the parent CR-CIR magma during magmatic fractionation (cf. Rollinson, 1993; White, 1991).

The possibility of early separation of these mineral phases from the CR-CIR parent magma has also been re-examined using incompatible versus compatible trace element log-log plots (after Cocherie 1986) (Fig. 9). This diagram indicates a drastic reduction of transition metals (Sc, Cr, Co, Ni etc.) with little increase in low D value elements (Rb, Cs, LREE, Hf, Ta, Th, U), during fractional crystallization of the magma. Also, in this diagram a nearly constant transition element concentration with a slight variation in low D elements indicates fusion process, while curvilinear trends indicate magma mixing. This geochemical technique has been widely used in literature to interpret the igneous process of formation of basaltic magmas (cf. Wilson, 1989, White, 1991). The compatible versus incompatible trace element diagrams (after Cocherie, 1986) have, therefore, been used in the present study to evaluate the liquid line of descent of the CR-CIR basalts (Fig. 9). The governing criterion for selection of elements in our plots is **their** very high degree**s** of variation**s** of these elements in **the** CR-CIR MORBs.

It is understood from k_D values of minerals that certain trace elements are characteristically withdrawn during fractionation of specific types of silicate minerals from the parent basaltic magma (Rollinson, 1993; Winter, 2001). For example, depletion of Ni is indicative of olivine (k_D= 5.9-29) fractionation from the melt; Cr fractionation indicates separation of clinopyroxene (k_D= 34) [also partly orthopyroxene (k_D= 10)] from the magma, and Sr is suggestive of withdrawal of plagioclase from the parent magma. The variations of compatible trace elements (Ni, Cr, Sr) against an incompatible trace element (Y) are, therefore, examined to evaluate the magmatic evolution of the CR-CIR MORBs (Fig. 9). The incompatible trace element Y is chosen because this element shows the maximum range of variation for present sample populations. Additionally, other incompatible trace element Zr is also considered in cases to confirm our observation (Fig. 10). In Y versus Ni plot, the most of the data of NCIR and SCIR-MORBs (except two) show a very gentle decrease of Ni with increasing Y(Fig. 9b), the CR and RTJ MORBs, however, do not show any variation of Ni with increasing Y within a narrow range (Fig. 9a). In Zr versus Ni plot, most of the data of the NCIR and SCIR MORBs describe a cluster of data rather any linear variation of Ni with increasing Zr (Fig. 10b). Most of the CR and RTJ data show almost no variation or slight increase in Ni with increasing Zr (Fig. 10a).

The Cr does not show any important variation with increasing Y (Figs. 9c, d). Although two data of the RTJ MORBs have relatively high Cr, while most of the data show near horizontal trend of variation for Cr with increasing Y. In Zr versus Cr plot, most of the data of the RTJ and SCIR; and all the CR MORBs show concentration at one point (Fig. 10c, d), the NCIR MORBs show almost no increase in Cr with increasing Zr. Little variations are observed in Y versus Ni plot for the RTJ MORBs, which are free of alteration, could be due to contamination of some unusual component (Price et al., 1986).

In Y versus Sr log-log plot, the most of the data of the RTJ MORBs along with the CR MORBs describe a co-linear horizontal trend of Sr with increasing Y (Fig. 9e). The RTJ MORBs also define an increasing trend for Sr with increasing Zr in Zr versus Sr log-log plot, whereas the CR MORBs form a cluster on this trend (Fig. 10e). Both the NCIR and SCIR MORBs show no variation of Sr with increasing Y (Fig. 9f). In Zr versus Sr log-log plot, the SCIR MORBs define an increasing linear trend for Sr with increasing Zr, while NCIR MORBs show no variation of Sr in this diagram (Fig. 10f).

The covariations between the incompatible trace element ratios and the least compatible elements of the two in the process identification plots (after White, 1991) are also examined for different CR-CIR MORBs (Fig. 11). These diagrams are usually used to discriminate the igneous process(s) involved: e.g. flat slope resulted due to crystallization of both fractional and equilibrium types while slope becomes steeper in case of partial melting and aggregate fractional melting**.**

In Zr versus Zr/Y plot (where Zr shows maximum variation for the CR-CIR MORBs), the CR and RTJ MORBs show different linear increasing trends for Zr/Y (from ~2.5 to 5) with increasing Zr (Fig. 11a). The NCIR and SCIR MORBs also show different linear increasing trends of Zr/Y (from ~ 2.5 to 5) with increasing Zr , although the SCIR MORBs data show much scatter of data (Fig. 11b). In Nb versus Nb/Y plot (where Nb shows minimum variation for CR-CIR MORBs), the CR and RTJ MORBs define different linear increasing trends for Nb/Y (from ~0.04 to 0.1) with increasing Nb (Fig. 11c). The NCIR and SCIR MORBs also show different linear increasing trends for Nb/Y (from ~0.05 to 0.6) with increasing Nb although scatter of data exists for SCIR MORBs (Fig. 11d).

6. Whole-rock isotope of CR-CIR MORB

The isotopic compositions of the different segments of CR-CIR MORBS collected from literature are compared with those of the Atlantic and Pacific MORBs in MORBs in $^{87}Sr/^{86}Sr$ versus $^{143}Nd/^{144}Nd$ plot (Fig. 12a**).** Here most of the Atlantic MORBs are plotted within an elliptic array, which shows a systematic linear decrease of $^{143}Nd/^{144}Nd$ with increasing $^{87}Sr/^{86}Sr$. The Pacific and CR-CIR MORBs

show slightly overlapping clusters of plots, which are well accommodated within the elliptical field of the Atlantic MORBs. While the Pacific MORBs show relatively primitive isotopic composition close to the depleted-mantle, the CR-CIR MORBs show evolved chemistry with relatively low $^{143}Nd/^{144}Nd$ and high $^{187}Sr/^{186}Sr$. Additionally, the most of the members of the CR-CIR MORBs show a more or less uniform $^{143}Nd/^{144}Nd$ ratios between ~0.5130 and 0.5131 with a few outlier exists among the NCIR MORBs. The variation in composition of the CR-CIR MORBs is mainly due to the variation in $^{87}Sr/^{86}Sr$ between ~0.7025 and 0.7035. Among the members of the CR-CIR MORBs, the least and most evolved $^{87}Sr/^{86}Sr$ compositions are shown by the CR and SCIR MORBs, respectively, while RTJ MORB show intermediate values. The NCIR MORBs, however, show the highest variation in $^{87}Sr/^{86}Sr$ ratios that extends from those of the CR to SCIR MORBs. When the compositions of the Indian Ocean Pelagic sediments (Ben Othman et al., 1989) is included in the $^{87}Sr/^{86}Sr$ versus $^{143}Nd/^{144}Nd$ plot, the average depleted-mantle and the pelagic sediment describe the two end members of a hyperbolic mixing trend where the CR-CIR MORBs are plotted on this trend in between these two end members but close to the D-mantle composition (Fig. 12b). The mixing trend definitely excludes EM1 [dehydrated and recrystallized oceanic basalt formed during subduction plus 5-10% marine pelagic sediment, Weaver, 1991], EM2 [dehydrated and recrystallized oceanic basalt formed during subduction plus 5-10% terrigenous sediments] and HIMU [recycled oceanic basalt without a significant presence of subducted sediments] sources (cf. Faure & Mensing, 2005, sec. 17.2).

In the $^{206}Pb/^{204}Pb$ versus $^{207}Pb/^{204}Pb$ plot, the CR and most of the NCIR and SCIR MORBs are plotted on or close to the mixing line between the average depleted mantle and the Indian Ocean Pelagic sediments, and this mixing line excludes the EM1, EM2 and HIMU (Fig. 12, c, e). The CR, NCIR and SCIR MORBs are closer to the average depleted-mantle composition on this mixing trend. Any possible mixing trend between the depleted mantle and EM2, however, excludes a majority of the CR-CIR data and cannot explain the distribution of the CR-CIR data in this diagram. The distribution of the RTJ MORBs, on the other hand, is different and these data describe an elliptical distribution, which is distributed between the EM1 and average depleted-mantle but have relatively high $^{207}Pb/^{204}Pb$. The Atlantic and Pacific MORBs, however, define another linear trend in this diagram that is completely different and oblique to the linear trend described by the CR-CIR MORBs (Fig. 12c).

The $^{206}Pb/^{204}Pb$ versus $^{208}Pb/^{204}Pb$ plot also includes two different linear trends. The first one between the depleted mantle and Indian Ocean Pelagic sediments, which includes the CR, NCIR and SCIR and some of the Atlantic MORBs, and excludes EM1, EM2 and HIMU averages (Fig. 12d).

The other trend, which is little oblique to the depleted-mantle-pelagic sediment trend, includes all of the Pacific and most of the Atlantic MORBs. Further observation on this diagram show that the CR, NCIR and SCIR MORBs, in fact, are distributed on a mixing trend between the depleted-mantle and upper continental crust end members, the pelagic sediments only represent an intermediate member on this linear trend (Fig. 12f). The compositional variation of the RTJ is mostly confined on a mixing trend between the depleted mantle and average lower continental crust.

7. Discussion

The detailed LIL, HFS elements and REE analyses show that the CR MORBs are compositionally akin to the RTJ MORBs, and both are close to the average N-MORB in composition (Figs. 6, 7). On the other hand, the NCIR and SCIR MORBs show significant compositional variations between the average N- and E-MORBs. These observations, therefore, suggests that the geochemical evolutions of the CR and RTJ-MORBs are different from those of the NCIR- and SCIR-MORBs, which could be due to the variation in igneous process(es) of formation and/or source rock compositions.

The processes involving crystallization of basalts from the CR-CIR are examined in more detail using the major and trace element chemistry. The CR-CIR MORBs do not show any important iron fractionation in bulk composition in comparison to the MAR and EPR MORBs (Fig. 5d). The other geochemical evidences against any bulk fractionation are indicated by no variations in (Na_2O+K_2O) and FeO^T/MgO with increasing SiO_2 in the CR-CIR MORBs (Fig. 5b, c). Relatively depleted LREE, and flat HREE (Fig. 7) in the CR-CIR MORBs (cf. Ray et al., 2011) also negate the role of any major fractionation during the evolution of these MORBs. In the compatible versus incompatible trace element log-log plots (after Cocherie, 1986), the CR-CIR MORBs show almost no variation or increasing proportion of compatible trace elements with increasing proportions of incompatible trace elements in most of the cases (Figs. 9, 10), which indicating partial melting dominated igneous process for the evolution of the CR-CIR MORBs. The variations of Ni, Cr and Sr in igneous rocks are sensitive to olivine, clinopyroxene and plagioclase fractionation respectively from the parent basic magma (cf. Rollinson, 1993; Winter, 2001). Our compatible versus incompatible trace element log-log plots (Figs. 9, 10), therefore, rule out any major role of fractionation of these minerals from the CR-CIR parent magma, although possibility of minor fractionation of olivine from the NCIR and SCIR cannot be ruled out by this diagram (Fig. 9b). Further confirmation against any major fractional crystallization for the CR-CIR MORBs comes from process identification plots (Fig. 11), where all of the members of the CR-CIR MORBs show increasing incompatible trace element ratios against the increasing proportions of the least

compatible trace element of the two suggesting partial melting dominated process for the evolution of the CR-CIR MORBs (cf. Winter, 2001).

In a partial melting dominated process, the variations in the incompatible trace element ratio plots (Fig. 8) could be indicative of possible involvement of enriched components, e.g., enriched-mantle, Oceanic Island Basalt (OIB)-like source or continental crust, in the depleted mantle source during the genesis of the NCIR and SCIR MORBs. However, this contamination appears to be least or absent for the CR and RTJ MORBs, which are plotted very close to the depleted N-MORB. The possibility of contamination of depleted mantle sources by enriched components is further substantiated by variation in compositions of the NCIR and SCIR MORBs in incompatible element spidergarm where MORBs from these two sectors show continuous variations between the average N- and E-MORBs (Fig. 6) and also in similar fashion in REE plots (Fig. 7). The Zr/Y versus Nb/Y diagram (Fig. 8d), on the other hand, suggests possible incorporation of deep mantle components during the genesis of the NCIR- and SCIR-MORBs. These various possibilities of contamination of the CR-CIR depleted mantle source by enriched materials have been discussed below with more sensitive isotope data.

The CR-CIR MORBs possess a distinct isotopic signature, mostly characterized by distinctly lower $^{143}Nd/^{144}Nd$, and higher $^{87}Sr/^{86}Sr$, $^{207}Pb/^{204}Pb$ and $^{208}Pb/^{204}Pb$ ratios compared to those of Atlantic and Pacific MORBs at a given $^{206}Pb/^{204}Pb$ ratio (Hart, 1984) (Fig. 12). These distinct isotopic characteristics of CR-CIR MORBs have been explained by several hypotheses, e.g. (a) Influence of Indian ocean hot spot sources, especially from the large long-lived Reunion or Kerguelen mantle plume (Storey et al.,1989); (b) continental mantle lithosphere incorporated prior to and/or during the breakup of Gondwana (Mahoney et al., 1992; Janney et al., 2005); (c) addition of recycled subducted altered oceanic crust and/or sediment (Dupre and Allegre, 1983; Rehkämper and Hofmann, 1997); (d) delaminated lower continental crust from cratonic Gondwanan lithosphere (Escrig et al., 2004; Hanan et al., 2004; Meyzen et al., 2005) and (e) subduction-modified mantle (Kempton et al., 2002).

In $^{87}Sr/^{86}Sr$ versus $^{143}Nd/^{144}Nd$ plots, the CR-CIR MORBs always plotted on or close to the mixing lines between the depleted mantle and pelagic sediment end members (Fig. 12a, b), and these lines never contain the average EM1, EM2 and HIMU indicating the least possibility of contamination of their respective depleted mantle sources with subducted oceanic crust with or without sediments. On the other hand, the mixing lines in $^{206}Pb/^{204}Pb$ versus $^{207}Pb/^{204}Pb$ plots (Fig. 12c, e) indicate possible contamination of the CR-CIR mantle source by continental crust because the pelagic sediments, one of the end members of these mixing lines, were derived from the upper

continental crust, and their isotopic compositions roughly represent the composition of the crust (Hofmann, 2003). This diagram also shows that the possible mixing line between the average depleted mantle and the EM2 excludes majority of the CR-CIR MORBs, and thus confirms the least possibility of contamination of the depleted mantle source by EM2 during the evolution of the CR-CIR MORBs, and the history of evolution of the RTJ MORBs appears to be different from that of the CR-CIR MORBs.

The best suited model for the evolutionary processes of the CR-CIR and RTJ MORBs is perhaps obtained from the $^{206}Pb/^{204}Pb$ versus $^{208}Pb/^{204}Pb$ plot (Fig. 12f). This diagram suggests that the RTJ MORBs were quite distinct from rest of the CIR and are derived from a depleted mantle that was contaminated by lower continental crust (LCC) and the amount of contamination could be ~21%. On the other hand, the CR, NCIR and SCIR MORBs completely lack the isotopic signature of triple-juction and were derived from a depleted mantle source that was variously contaminated by upper continental crust (UCC). The amounts of contaminations are least for the CR and NCIR MORBs and the value is close to ~19%, and it is highest for the SCIR MORBs, which is ~32%. Escrig et al. (2004) also showed that the isotopically most contaminated part of CIR lies between latitudes ~15^{o}S and 22^{o}S, which in fact include the major part of the SCIR (Fig. 1). The MORBs from this sector, in general, have higher $^{206}Pb/^{204}Pb$ (~4%), $^{87}Sr/^{86}Sr$ (~0.1%) and $^{187}Os/^{188}Os$ (~2.7%) and lower $^{143}Nd/^{144}Nd$ (~0.03%) compared to the rest of the sectors of CR-CIR.

There are two different views existing on the nature of contamination of the CIR mantle (cf. Escrig et al., 2004), a majority of workers opined that recycled continental lithosphere either as old sub-continental lithosphere or as sediments associated with oceanic crust are the main contaminants (Hamelin and Allegre, 1985; Hamelin et al., 1985/86; Michard et al., 1986; Price et al., 1986; Dosso et al., 1988; Mahoney et al., 1989; Mahoney et al., 1992; Rehkämper and Hofmann, 1997). Others, however, suggest that delamination of lower continental crust was the main source of this contamination (Escrig et al., 2004). Our study suggests both of these models could be correct except the concept of contamination of CR-CIR depleted mantle solely by subducted oceanic crust (e.g. HIMU) because the isotopic plots (Fig. 12) never suggest this possibility. Our present compilation on the $^{206}Pb/^{204}Pb$ versus $^{208}Pb/^{204}Pb$ plot (Fig. 12f) further suggests that the depleted mantle source of the RTJ MORBs was contaminated by the lower continental crust, whereas the mantle source of the CIR MORBs was contaminated by the upper continental crust at various level, which is maximum at the southern CIR and minimum at the northern CIR and CR. We have computed the possible composition of the contaminated mantle sources for the CR-CIR MORBs (Table S-1, Fig. S2 in supplementary materials). The mantle sources in bulk compositions are komatiitic basalt wherein

composition of MgO was between ~26-31 wt% and Mg# ~ 0.87. The Al_2O_3/ TiO_2 ratios vary between ~21-26 indicating the source rock is Al-undepleted komatiite. The CaO/Al_2O_3 ratios are relatively low and vary between ~0.48 and 0.67. The most important effect of crustal contamination is to enrich the depleted mantle source in Rb (~20 to 400 times), Ba (~20-100 times), La and Ce (~5-30 times) and Ta (~20 times).

The actual mechanism accounting this mantle contamination is still a matter of debate, although studies on the south Atlantic ridge suggest that the contamination of upper mantle by lower continental crust could have been resulted during major Gondwana break up at the late Jurassic-early Cretaceous period (~145 Ma) (Kamenestsky et al., 2001). A similar idea can be also employed for the Indian Ocean because the Gondwana break up is the only known super major tectonic event that pre-dated the commencement of spreading along the Indian Ocean Ridge system during Eocene (~56 Ma) (Norton and Sclater, 1979) and isolated continental fragments that could be the result of Gondwana fragmentation are more numerous in Indian Ocean in comparison to the Atlantic and Pacific Oceans (Weis et al., 2001). Rehkämper and Hofmann (1997) in their geochemical model showed that the age of the pelagic sediments that could have contaminated the depleted mantle source of the CIR MORBs was > 125 Ma, which in fact is time equivalent to the third stage of Gondwana break up during 155-135 Ma, when a mega fracture system across the Gondwana was developed through this area that extended from the Tethys past the Lebombo area of South Africa to the Proto-Pacific ocean, and strike slip movement along this system split the Gondwana into two plates, the East Gondwana (Antractica, Madagascar, India and Australia) and West Gondwana (South America and Africa) (Watkeys, 2002; 2006). This mega fracture is thought to be one of the transform faults, the Davie Fracture Zone, that were related to onset of seafloor spreading in the Somali basin during this period (Scotese et al., 1988). In the subsequent period (~135-115 Ma) the movement along this mega-fracture system resulted drifting of the East and West Gondwana blocks. It appears that the Indian Ocean upper mantle, close to the present position of RTJ, was first contaminated by delamination of lower continental crust during the movement of this mega fracture. During the subsequent movement of the Indian sub-continent between the 115-90 Ma, the SCIR mantle region was contaminated by the lower part of the upper continental crust. The role of the Reunion plume on the evolution of the CR-CIR MORBs is perhaps least significant because on-axis CIR MORBs between 18^o S and 20^o S latitudes do not show any influence of this plume in Pb-isotopic and highly incompatible element trends (Nauret et al., 2006).

The major and trace element compositional variations of the NCIR MORBs were initially thought to be due to crystal fractionation in our previous study (Ray et al., 2007). Our detail

investigation in present observation suggests that these variations could be due to various contamination of the depleted mantle source by the Indian Ocean pelagic sediments.

8. Conclusion

(a) In trace element geochemistry [e.g., LIL and REE spidergrams and $(La/Sm)_N$ ratio etc.], the CR MORBs are compositionally similar to the RTJ MORBs, both of which are closely resembling to the average N-MORB composition. The MORBs from the NCIR and SCIR significantly vary in composition between average N- and E-MORBs.

(b) Major and trace element modeling suggests that the CR-CIR MORBs were evolved by partial melting dominated process.

(c) The isotopic compositional variations of the CR-CIR MORBs, particularly in $^{206}Pb/^{204}Pb$ versus $^{208}Pb/^{204}Pb$ diagram, suggest that their depleted mantle source has been variously contaminated by the lower and upper continental crustal components. The RTJ MORBs were derived from a mantle source that was contaminated by ~21% lower continental crust, where as the source mantle of the CR and NCIR MORBs contains upper continental crustal components upto ~19% and the value is maximum for the SCIR mantle source, which is ~32%. The contaminated mantle sources are similar to Al-depleted Komatiite basalt in composition that are significantly enriched in Rb, Ba, La and Ce with reference to depleted mantle.

(d) This contamination of the Indian Ocean mantle was perhaps related to the third stage of Gondwana break up during 155-135 Ma when strike slip movement along a mega fracture, belonging to the Davie Transform Faults within the Somali basin, split the Gondwanaland into the East and West Gondwana plates.

Acknowledgement

We thank the Ministry of Earth Sciences, New Delhi, India, for the availability of the ORV Sagar Kanya, the scientific party and crew of the maiden cruise, for assistance during sample collection and the National Centre for Antarctic and Ocean Research (NCAOR), Goa, India, for allotting the cruise as schedule and for logistics. We are obliged to Directors, NCAOR and NIO, Goa, India, for constant encouragement during the progress of this work. Especial thanks to M. K. Watkeys and H. Kumagai for constructive comments on the early version of the manuscript. Constructive reviews by S. Arai and J.G. Liou are greatly appreciated. The second author (S.M.) is thankful to the University of KwaZulu-Natal, Durban, South Africa, for Competitive Research Grant (RG-41) for this work.

References

Arevalo, R (Jr.)., McDonough, W. F., 2010. Chemical variations and regional diversity observed in MORB. Chem. Geol. 271, 70-85.

Armienti, P., Gasperini, D., 2007. Do we really need mantle components to define mantle compositions? J. Petrol. 48, 693-709.

Balaram, V., Gnaneshwara Rao, T., Anjaiah, K.V., 1999. International proficiency tests for analytical geochemistry laboratories: an assessment of accuracy and precision in routine geochemical analysis. J. Geol. Soc. Ind. 53, 417–423

Banerjee, R., Iyer, S.D., 1991. Petrography and chemistry of basalts from the Carlsberg Ridge. J. Geol. Soc. Ind. 38, 369 – 386.

Banerjee, R., Iyer, S.D., 1993. A note on the sulphide-oxide mineralization in Carlsberg Ridge. J. Geol. Soc. Ind. 42, 579-584.

Banerjee, R., Iyer, S.D., 2003. Genetic aspects of basalts from the Carlsberg Ridge. Curr. Sci. 85, 299-305.

Ben Othman, D. White, W.M., Patchett, J., 1989. The geochemistry of marine sediments, island arc magma genesis, and crust-mantle recycling. Earth Planet. Sci. Lett. 94, 1-21.

Briais, A., 1995. Structural analyses of the segmentation of the Central Indian Ridge between 20°30′S and 25°30′S. Mar. Geophys. Res. 17, 431-467.

Chaubey, A.K. Bhattacharya, G.C. Murthy, G.P.S., Desa, M., 1993. Spreading history of Arabian sea: some new constraints. Mar. Geol. 112, 343-352.

Christie, D.M., West, B.P., Pyle, D.G., Hanan, B., 1998. Chaotic topography, mantle flow and mantle migration in the Australian-Antarctic Discordance. Nature 394, 637-644.

Cocherie, A., 1986. Systematic use of trace element distribution patterns in log–log diagrams for plutonic suites. Geochim. Cosmochim. Acta 50, 2517–2522.

Condie, K.C., 2003. Incompatible element ratios in oceanic basalts and komatiites: Tracking deep mantle sources and continental growths with time. Geochem. Geophys. Geosyst. 4, doi: 10.1029/2002GC000333.

Donnelly, K.E., Goldstein, S.L., Langmuir, C.H., Spiegelman, M., 2004. Origin of enriched ocean ridge basalts and implications for mantle dynamics. Earth Planet. Sci. Lett. 226, 347-366.

Dosso, L., Bougauit, H., Beuzart, P., Clavez, J-Y., Joron, J.L., 1988. The geochemical structure of the South-East Indian Ridge. Earth Planet. Sci. Lett. 88, 47-59.

Drolia, R.K., Iyer, S.D., Chakraborty, B., Kodagali, V., Ray, D., Misra, S., Andrade, R., Sarma, K.V.L.N.S., Rajasekhar, R.P., Mukhopadhyay, R., 2003. The Northern Central Indian Ridge: Geology and tectonics of fracture zones-dominated spreading ridge segments. Curr. Sci. 85, 290-298.

Drolia, R.K., DeMets, C., 2005. Deformation in the diffuse India-Capricorn-Somalia triple junction from a multibeam and magnetic survey of the northern Central Indian Ridge, 3ºS-10ºS, Geochem. Geophys. Geosyst. 6, doi 2005GC000950.

Dupre, B., Allegre, C.J., 1983. Pb–Sr isotope variations in Indian Ocean basalts and mixing phenomena. Nature 303, 142–146.

Escrig, S., Capmas, F., Dupre, B., Allegre, C.J., 2004. Osmium isotopic constraints on the nature of the DUPAL anomaly from Indian mid-ocean-ridge basalts. Nature 431, 59–63.

Faure, G., Mensing, T.M., 2005. Isotopes: Principles and applications (3rd edition). Wiley, 897 pp.

Fitton, J.G., Saunders, A.D., Norry, M.J., Hararson, B.S., Taylor, R.N., 1997. Thermal and chemical structure of the Iceland plume. Earth Planet. Sci. Lett. 153, 197-208.

Hamelin, B., Allegre, C.J., 1985. Large-scale regional units in the depleted uppermantle revealed by an isotope study of the southwest Indian Ridge. Nature 345, 196-199.

Hamelin, B., Dupre, B., Allegre, C.J., 1986. Pb-Sr-Nd isotopic data of Indian Ocean ridges: new evidence of large-scale mapping of mantle heterogeneities. Earth Planet. Sci. Lett. 76, 286-296.

Hamilton, W.B., 2011. Plate tectonics began in Neoproterozoic time, and plumes from deep mantle have never operated. Lithos 123, 1-20.

Hanan, B.B., Blichert-Toft, J., Pyle, D.G., Christie, D.M., 2004. Contrasting origins of the upper mantle revealed by hafnium and lead isotopes from the Southeast Indian Ridge. Nature 432, 91–94.

Hart, S.R., 1984. A large-scale anomaly in the Southern Hemisphere mantle. Nature 309, 753–757.

Hekinian, R., 1968. Rocks from the mid-ocean ridge in the Indian Ocean. Deep-Sea Res. 15, 195-213

Hekinian, R., 1982. Petrology of the Ocean floor, Elsevier, Amsterdam, 393 pp.

Hemming, S.R., McLennan, S.M. 2001., Pb isotope compositions of modern deep sea turbidities. Earth Planet. Sci. Lett. 184, 489-503.

Herzig, P.M., Pluger, W.L., 1988. Exploration for hydrothermal activity near the Rodriguez Triple Junction, Indian Ocean. Canad. Mineral. 26, 721-736

Hofmann, A.W., 2003. Sampling mantle heterogeneity through oceanic basalts: isotopes and trace elements, In: Carlson, R.W. (Ed.) The mantle and Core. Treatise on Geochemistry, Elsevier-Pergamon, Oxford, 2, pp 61-101.

Honsho, C., Tamaki, K., Fujimoto, H., 1996. Three-dimensional magnetic and gravity studies of the Rodriguez Triple Junction in the Indian Ocean. J. Geophys. Res. 101, 15837-15848.

Humler, E., Whitechurch, H. 1988. Petrology of basalts from the Central Indian Ridge (lat 25º23′S, long 70º04′E): estimates of frequencies and fractional volumes of magma injections in a two-layered reservoir. Earth Planet. Sci. Lett. 88, 169-181.

Iyer, S.D., Banerjee, R., 1993. Mineral chemistry of Carlsberg Ridge basalts. Geo-Mar. Lett. 13, 153-158.

Iyer, S.D., Ray, D., 2003. Structure, tectonic and petrology of mid-oceanic ridges and the Indian Scenario, Curr. Sci. 85, 277-289.

Janney, P.E., Le Roex, A.P., Carlson, R.W. 2005. Hafnium Isotope and Trace Element Constraints on the Nature of Mantle Heterogeneity beneath the Central Southwest Indian Ridge (13ºE to 47ºE). J. Petrol. 46, 2427-2464.

Kamanetsky, V.S., Mass, R., Sushchevskaya, N.M., Norman, M.D., Cartwright, I., Peyve, A.A., 2001. Remnants of Gondwana continental lithosphere in oceanic upper mantle: Evidence from the South Atlantic Ridge. Geology 29, 243-246.

Kamesh Raju, K.A., Kodagali, V.N., Fujimoto, H., 1998. Three dimensional gravity and magnetic studies over a segment of the Carlsberg ridge [abs], 35th Annual convention and meeting on Continental Margins of India-Evolution, Processes and Potentials, Indian Geophysical Union, held at NIO, Goa. Nov 18-20, p 29.

Kamesh Raju, K.A., Chaubey, A.K., Amarnath, D., Mudholkar, A., 2008. Morphotectonics of the Carlsberg Ridge between 62˚20/ and 66˚20/E, northwest Indian Ocean. Mar. Geol. 252, 120-128.

Kempton, P.D., Pearce, J.A., Barry, T.L., Fitton, J.G., Langmuir, C., Christie, D.M., 2002. Sr–Nd–Pb–Hf isotope results from ODP Leg 187: evidence for mantle dynamics of the Australian–Antarctic Discordance and origin of the Indian MORB source. Geochem. Geophys. Geosyst. 3, doi 2002GC000320.

Mahoney, J.J., Natland, J.H., White, W.M., Poreda, R., Bloomer, S.H., Fisher, R.L., Baxter, A.N., 1989. Isotopic and geochemical provinces of the western Indian Ocean spreading centers. J. Geophys. Res. 94, 4033-4052.

Mahoney, J.J., le Roex, A.P., Peng, Z., Fisher, R.L., Natland, J.H., 1992. Southwestern limits of Indian Ocean Ridge mantle and the origin of low $^{206}Pb/^{204}Pb$ mid-ocean ridge basalts: isotope systematics of the Southwest Indian Ridge (17º–50ºE). J. Geophys. Res. 97**,** 19771–19790.

Mahoney, J.J., Graham, D.W., Christie, D.M., Johnson, K.T.M., Hall, L.S., Vonderhaar, D.L., 2002. Between a hotspot and a coldspot: Isotopic variation in the southeast Indian Ridge asthenosphere, 86°E-118°E. J. Petrol. 43, 1155-1176.

McDonough, W.F., Sun, S.S., 1995. The composition of the Earth, Chem. Geol. 120, 223-253.

McKenzie, D.P., Sclater, J.G., 1971. The evolution of the Indian Ocean since the late Cretaceous. Geophys. J. Royal Astronom. Soc. 25, 437-528.

McLennan, S.M., 2001. Relationships between the trace element composition of sedimentary rocks and upper continental crust. Geochem. Geophys. Geosyst. 2, doi: 2000GC000109.

Meyzen, C., Toplis, M., Humler, E. Ludden, J., Mevel, C., 2003. A discontinuity in mantle composition beneath the Southwest Indian ridge. Nature 421, 731-733.

Meyzen, C.M., Ludden, J.N., Humler, E., Luais, B., Toplis, M.J., Mevel, C., Storey, M., 2005. New insights into the origin and distribution of the DUPAL isotope anomaly in the Indian Ocean

mantle from MORB of the Southwest Indian Ridge. Geochem. Geophys. Geosyst. 6, doi 2004GC000798.

Michard, A., Montigny, R., Schlich, R. 1986. Geochemistry of the mantle beneath the Rodriguex triple junction and the South East Indian Ridge. Earth Planet. Sci. Lett. 78,104-114.

Mudholkar, A.V., Kodagali, V.N., Kamesh Raju, K.A., Valsangkar, A.B., Ranade, G.H., Ambre, N.V., 2002. Geological and geophysical observations along a segment of slow spreading Carlsberg Ridge. Curr. Sci. 82, 2982-2989.

Mukhopdhyay, R., Iyer, S.D., 1993. Petrology of tectonically segmented Central Indian Ridge. Curr. Sci. 65, 623-628.

Munschy, M., Schlich, R., 1989. The Rodriguez Triple Junction (Indian Ocean): Structure and evolution for the past one million years. Mar. Geophys. Res. 11, 1-14.

Murton, B.J., Tindle, A.G., Milton, J.A., Sauter, D., 2005. Heterogeneity in southern Central Indian Ridge MORB: Implications for ridge-hot spot interaction. Geochem. Geophys. Geosyst. 6, doi 2004GC000798.

Natland, J.H., 1991. Indian Ocean crust, In: Floyd, P.A. (Ed.). Oceanic Basalts, Blackie and Sons, Glasgow, UK, pp. 289-310

Nauret, F., Abouchami, W., Galer, S.J.G., Hofmann, A.W., Hemond, C., Chauvel, C., Dyment, J., 2006. Correlated trace element-Pb isotope enrichments in Indian MORB along 18-20ºS, Central Indian Ridge, Earth Planet. Sci. Lett. 245, 137-152.

Nesbitt, H.W., Wilson, R.E., 1992. Recent chemical weathering of basalts. Am. J. Sci. 292 (10), 740-777.

Newsom, H.E., Misra, S.**,** Wright, S.P., Muttik, N., 2010. Contrasting alteration and enrichment of mobile elements during weathering of basaltic ejecta and ancient soils at Lonar crater, India. 41st Lunar Planet. Sci. Conf., abs. No. 2210 (CD-ROM).

Norton, I.O., Sclater, J.G., 1979. A model for the evolution of the Indian Ocean and the break up of Gondwanaland. J. Geophys. Res. 84, 6803-6830.

Parson, L.M., Patriat, P., Searle, R.C., Briais, A., 1993. Segmentation of the Central Indian Ridge between 12º12'S and the Indian Ocean Triple Junction. Mar. Geophys. Res. 15, 265-282.

Peach, C.L., Mathez, E.A., Keays, R.R., 1990. Sulphide melt-silicate melt distribution coefficients for noble metals and other chalcophile elements as deduced from MORB: implications for partial melting. Geochim. Cosmochim. Acta 54, 3379-3389.

Petrological Database of Ocean floor, website: http://beta.petdb.ciesin.columbia.edu/index.jsp

Pluger, W.L. and cruise participants. 1988. Fahrtbericht SO-28 and Wissenschaftlicher Bericht GEMINO-I: Geothermal Metallogenesis Indian Ocean, 274pp.

Presnall, D.C., Hoover, J.D., 1987. High pressure phase equillibrium constrints on the origin of mid-ocean ridge basalts. In: Mysen, B.O. (Ed.) Magmatic Processes: Physico chemical Principles. Geochemical Society of London, 1, pp 75-89 (Special Publication).

Price, R.C., Kennedy, A.K., Riggs-Sneeringer, M., Frey, F.A., 1986. Geochemistry of basalts from the Indian ocean triple junction: implications for the generation and evolution of Indian Ocean ridge basalts. Earth Planet. Sci. Lett. 78, 379-396

Ramana, M.V., Ramprasad, T., Kamesh Raju, K.A., Desa, M. 1993. Geophysical studies over a segment of the Carlsberg Ridge, Indian Ocean. Mar. Geol. 115, 21-28.

Ray, D., Iyer, S.D., Banerjee, R., Misra, S., Widdowson, M., 2007. Petrology and Geochemistry of basalts from the Northern Central Indian Ridge (3-11ºS): implications for the evolution of MORB. Acta Geol. Sin. (English edition) 81, 99-112.

Ray, D., Banerjee, R., Iyer, S.D., Basavalingu, B., Mukhopadhyay, S., 2009. Glass and mineral chemistry of Northern Central Indian Ridge basalts: compositional diversity and petrogenetic significance. Acta Geol. Sin. (English edition) 83, 1122-1135.

Ray, D., Misra, S., Banerjee, R., Weis, D., 2011. Geochemical implications of gabbro from slow-spreading Northern Central Indian Ocean Ridge, Indian Ocean. Geol. Mag. 148(3), 404-422.

Rehkamper, M., Hofmann, A.W., 1997. Recycled ocean crust and sediment in Indian Ocean MORB. Earth Planet. Sci. Lett. 147, 93-106

Rollinson, H.R., 1993. Using geochemical data: Evaluation, presentation, interpretation. Longman, England, 352 pp.

Royer, J.Y., Sandwell, D.T., 1989. Evolution of the eastern Indian ocean since the late Cretaceous-constraints from Geosat altimetry. J. Geophys. Res. 94, 13, 755-13, 782.

Royer, J.Y., Gordon, R.G., DeMets, C., Vogt, P.R., 1997. New limits on the motion between India and Australia since chron 5 (11 ma) and implications for lithospheric deformation in the equatorial Indian Ocean. Geophys. J. Int. 129**,** 41-53.

Salters, V.J.M., Stracke, A., 2004. Composition of the depleted mantle. Geochem. Geophys. Geosyst. 5, doi 10.1029/2003GC000597.

Sauter, D., Nafziger, J.-M., Whitechurch, H., Munschy, M., 1996. Segmentation and morphotectonic variations of the Central Indian Ridge (21°10′S-22°25′S). J. Geophys. Res. 101, 20,233-20,256.

Schlich, R., 1982. The Indian Ocean: Asismic ridges, spreading centres and oceanic basins. In: Nairn, A.E.M., Stehli, F.G. (Eds.), The Ocean basin and margins, Plenum Press, New York, 6, pp 51-147.

Schilling, J.G., Zajhare, M., Evans, R., Johnson, T., White, W., Devine, J.D., Kingsley, R., 1983. Petrologic and geochemical variations along the Mid-Atlantic Ridge from 29˚N to 73˚N, Am. J. Sci. 283, 510-586.

Scotese, C.R., Gahagan, L.M., Larson, R.L., 1988. Plate tectonic reconstructions of the Cretaceous and Cenizoic ocean basins. Tectonophysics 155, 27-48.

Storey, M., Saunders, A.D., Tarney, J., Gibson, I.L., Norry, M.J., Thirlwall, M.F., Leat, P., Thompson, R.N., Menzies, M.A., 1989. Contamination of Indian Ocean asthenosphere by the Kerguelen–Heard mantle plume. Nature 338, 574–576

Subbarao, K.V., Hedge, C.E. 1973. K, Rb, Sr and $^{87}Sr/^{86}Sr$ in rocks from the Mid-Indian Ocean Ridge. Earth Planet. Sci. Lett. 18, 223-228.

Subbarao, K.V., Reddy, V.V., Hekinian, R., Chandrasekharam, D., 1977. Large ion lithophile elements and Sr and Pb isotopic variam the Indian Ocean. In: (Heirtzler J.R., Bolli, J.R., Davies, T.A., Saunders, J.B., Sclater, J.G. (Eds.), Indian Ocean Geology and Biostratigraphy, American Geophysical Union, Lithocrafters, Washington DC, pp. 259-278.

Subbarao, K.V., Kempe, D.R.C., Reddy, V.V., Reddy, G.R., Hekinian, R., 1979. Review of the geochemistry of Indian and other oceanic rocks. In: Ahrens, L.H. (Ed.), Origin and Distribution of the Elements Pergamon Press, Oxford, pp. 367-399.

Sun, S.S., McDonough, W.F. 1989. Chemical and isotope systematics of ocean basalts: implications for mantle composition and processes, In: Saunders, A.D., Norry, M.J. (Eds.), Magmatism in the Ocean Basins. Geological Society of London 42, pp. 313-345 (Special Publication).

Watkeys, M.K., 2002. Development of the Lebombo rifted volcanic margin of southeast Africa. Geological Society of America 362, pp. 27-46 (Special Publication).

Watkeys, M.K., 2006. Gondwana break-up: A South African perspective. In: Johnson, M.R., Anhaeusser, C.R., Thomas, R.J. (Eds.), The Geology of South Africa. The Geological Society of South Africa, Johannesburg, and Council for Geoscience, Pretoria, pp. 531-539.

Weaver, B.L., 1991. The origin of ocean island end-member compositions: trace element and isotopic constraints, Earth Planet. Sci. Lett. 104, 381-397

Weis, D., Ingle, S., Damasceno, D., Frey, F.A., Nicolaysen, K., Barling, J., Leg 183 Shipboard Scientific Party, 2001. Origin of continental components in Indian Ocean basalts: Evidence from Elan Bank (Kerguelen Plateau, ODP Leg 183, Site 1137). Geology 29, 147-150.

White, W.M., 1991. Trace elements in igneous processes, In: Dasch, E.J. (Ed.), Encyclopedia of Earth Sciences. Macmillan, New York, 1, pp. 256-307.

Wilson, M., 1989. Igneous Petrogenesis-a Global Tectonic Approach. Chapman and Hall, London, 466 pp.

Winter, J.D., 2001. A Introduction to Igneous and Metamorphic Petrology, Printice Hall, New Jersey, 697 pp.

Table Captions

Table 1: Major Oxide and Trace element data of CR MORBs.

Table 2: Summary on available modal data on CR, NCIR, SCIR and RTJ MORBs.

Table 3: Comparative major oxide compositions of CR, NCIR, SCIR and RTJ MORBs.

Figure Captions

Fig. 1a. Map showing Indian Ocean Ridge systems. Known dredge locations have also shown as four different symbols in four ridge segments. Symbols: CR: Carlsberg ridge, NCIR: Northern Central Indian Ridge, SCIR: Southern Central Indian Ridge and RTJ: Rodriguez Triple Junction. Inset Fig. 1b (as shown in satellite bathymetry) showing present dredge locations (e.g. dr 01 and dr 02) along the CR. Ridge-axis and traces of magnetic chron are drawn following Kamesh Raju et al., 2008.

Fig. 2. Photomicrographs of CR basalts showing a. quenched plagioclase laths in glassy MORB, b. olivine and plagioclase as glomeroporphyritic aggregates, c. twinning and zoning in plagioclase phenocryst and d. 'skeletal' plagioclase grains. e. melt inclusion in plagioclase phenocryst and f. 'swallow-tailed' olivine in variolitic zone. Scale bar as shown in figs.

Fig. 3. Ranges of Plagioclase (An wt%) and olivine composition (Fo wt%) of different morphologies of CR, NCIR, SCIR and RTJ MORB. Data source: CR: Iyer and Banerjee (1993); NCIR: Ray et al. (2009); SCIR: Sauter et al. (1996) and RTJ: Price et al. (1986).

Fig. 4. Ternary $CaO+Na_2O+K_2O+MgO$ (CNKM) -FeO^T-Al_2O_3 plots (after Nesbit and Wilson, 1992) for CR-CIR MORBs, Grey lines represents the Feldspar (Fel) line. Individual plots of CR, NCIR, SCIR and RTJ MORBs are shown in insets. Data source: CR: Banerjee and Iyer (2003); NCIR: Ray et al. (2007); SCIR: Murton et al. (2005); Nauret et al. (2006); RTJ: Price et al. (1986), additional data taken from PetDB.

Fig. 5. Binary plots for major oxides of CR-CIR MORBs in (a) Na_2O (wt%) versus TiO_2(wt%), (b) Na_2O+K_2O versus SiO_2 (wt%), and (c) FeO^T/MgO versus plots, and d) Ternary CaO-MgO-FeO^T plot of CR-CIR MORBs. Data source as in figure 4, EPR and MAR data from www.geokem.com/ORB-Oceanic-summary.html.

Fig. 6. Primitive mantle normalized multivariate plots (spiderdiagrams) for CR-CIR MORBs. Primitive mantle, average N and E-MORBs data from Sun & McDonough (1989). Grey lines and dark lines represent two CR dredge samples dr 01 and dr 02 respectively. Data Source: CR: present data in table 1; NCIR: Ray et al. (2007); SCIR: Murton et al. (2005), Nauret et al. (2006); RTJ : Price et al. (1986) and PetDB.

Fig. 7 (a-d) Chondrite normalised REE spiderdiagrams for CR-CIR MORBs. Chondrite nomalised data from McDonough and Sun (1995), symbols and data sources as in figure 6.

Fig. 8. Binary plots of CR-CIR MORBs in (a) Mg# versus $(La/Sm)_N$, (b) $(La/Yb)_N$ versus $(Nb/Yb)_N$, (c) $(La/Yb)_N$ versus $(Ba/Yb)_N$ and (d) Zr/Y versus Nb/Y diagrams. Boundary line between plume and non-plume sources in figure 8d from Fitton et al (1997) and end member compositions from Condie (2003), subscript 'N' in some trace element ratios represents chondrite (after McDonough and Sun, 1995) normalized value. Symbols and data sources as in figure 6, average N and E-MORB data from Sun and McDonough (1989).

Fig. 9. Binary log-log plots (a, b, c, d, e, f) of compatible (Ni, Cr and Sr) versus incompatible trace elements (Y) (after Cocherie, 1986) for the CR-CIR MORBs. Symbols and data sources as in figure 6. Arrowed lines indicate the trend of variation of the compatible elements with increasing incompatible elements.

Fig. 10. Binary log-log plots (a, b, c, d, e, f) of compatible (Ni, Cr and Sr) versus incompatible trace elements (Zr) (after Cocherie, 1986) for the CR-CIR MORBs. Symbols and data sources as in figure 6. Arrowed lines indicate the trend of variation of the compatible elements with increasing incompatible elements. Note the variations of Ni, Cr and Sr values of RTJ MORBS between figures 9 (a,c,e) and 10 (a,c,e). These variations are due to variations of corresponding data of Ni, Cr and Sr against Zr and Y in literature (Price et al., 1986 and PetDB).

Fig. 11. Binary plots (a, b, c, d) of incompatible trace element ratios (Zr/Y and Nb/Y) against the least compatible elements of the two (Zr and Nb) (after White, 1991) for the CR-CIR MORBs. Symbols and data sources as in figure 6. Arrowed lines indicate the trend of variation of incompatible trace element ratios with increasing proportion of the least compatible elements of the two.

Figs. 12. Binary plots of CR-CIR MORBs in (a, b) $^{143}Nd/^{144}Nd$ versus $^{87}Sr/^{86}Sr$, (c, e) $^{207}Pb/^{204}Pb$ versus $^{206}Pb/^{204}Pb$, and (d, f) $^{208}Pb/^{204}Pb$ versus $^{206}Pb/^{204}Pb$ diagrams along with different crustal and mantle end members. Symbols of CR-CIR MORBs as in figure 6, the field of IORS MORBs in figure 12a is shown by an ellipse drawn in solid line, the fields of RTJ MORBs in figure 12c and 12e are shown by ellipses drawn in dotted lines. Data source: CR and NCIR: Rehkamper and Hofmann (1997); SCIR: Nauret et al. (2006); RTJ 1: Price et al. (1986), additional data from CIR (small open circle) and RTJ (as denoted RTJ 2: small grey triangles): Escrig et al. (2004); Indian Ocean Pelagic sediments (open triangle): Ben Othman et al. (1989), D-mantle (open diamond): Hart (1984); HIMU (solid square), EM1 (solid circle) and EM2 (bold open circle): Armienti and Gasperini (2007), Lower continental crust (LCC, grey square): Escrig et al. (2004), Upper continental crust (UCC, open square): Hemming and McLennan (2001); Atlantic (light grey square) and Pacific (deep grey square with black boundary) MORBs : PetDB.

Table 1

Sample no.	dr-1a	dr-1b	dr-1c	dr-1d	dr-1e	dr-1f	dr-1g	dr-1h	dr-1i	dr-1j
SiO_2(wt%)	51.38	50.82	51.01	50.96	51.2	50.79	51.15	51.21	50.64	50.87
TiO_2	1.12	1.45	1.51	1.5	1.49	1.73	1.13	1.46	1.78	1.47
Al_2O_3	15.5	15.83	15.38	15.32	15.61	14.83	15.48	15.53	14.74	15.63
Fe_2O_3	9.14	9.86	10.12	10.17	9.86	10.97	9.29	9.9	11.16	10
MnO	0.17	0.17	0.18	0.18	0.18	0.18	0.18	0.18	0.19	0.18
MgO	8.49	7.97	8.09	8.21	8.08	8.04	8.39	8.16	7.89	7.97
CaO	12.07	11.6	11.51	11.51	11.57	10.88	12.12	11.73	10.74	11.58
Na_2O	2.47	2.42	2.45	2.47	2.58	2.56	2.4	2.51	2.55	2.41
K_2O	0.09	0.12	0.12	0.12	0.16	0.15	0.1	0.12	0.14	0.12
P_2O_5	0.1	0.14	0.14	0.14	0.14	0.16	0.1	0.14	0.17	0.14
Total	100.53	100.38	100.51	100.58	100.87	100.29	100.34	100.94	100	100.37
Mg#	0.65	0.62	0.61	0.62	0.62	0.59	0.64	0.62	0.58	0.61
Sc (ppm)	35.97	37.68	35.95	35.75	38.17	39.35	38.09	37.94	37.70	36.68
V	282.67	313.17	276.90	277.29	303.16	296.63	263.16	258.83	265.88	293.46
Cr	263.99	290.78	257.06	280.48	342.66	303.01	395.43	386.94	404.74	296.01
Co	43.284	44.733	42.622	40.287	44.68	43.981	44.552	43.054	44.701	43.132
Ni	89.80	117.43	88.59	89.10	122.06	109.23	108.27	100.79	117.04	108.70
Cu	71.73	75.13	70.97	68.40	81.76	84.48	77.57	73.38	93.34	71.22
Zn	108.04	124.96	117.02	108.48	122.61	121.09	94.84	90.64	92.82	118.36
Ga	16.36	16.68	16.01	16.61	16.53	16.41	15.59	15.42	15.48	16.36
Rb	3.14	1.08	4.81	4.14	1.09	1.05	0.92	0.80	0.75	1.19
Sr	124.19	126.08	122.03	114.90	106.29	105.12	111.91	107.45	109.56	107.27
Y	34.32	40.01	34.42	36.24	37.66	37.18	29.54	29.54	28.93	36.55
Zr	103.00	136.60	106.73	106.33	110.75	110.62	77.25	81.42	77.48	106.18
Nb	2.46	3.85	2.78	2.67	3.60	3.58	2.14	2.18	2.11	3.23
Cs	0.17	0.02	0.23	0.21	0.03	0.02	0.03	0.04	0.02	0.03
Ba	14.06	15.28	12.09	14.55	16.35	12.37	13.52	12.95	17.33	16.33
La	3.62	4.71	3.54	3.55	3.82	3.72	2.76	2.70	2.71	3.81
Ce	10.9	14.27	10.93	10.77	11.67	11.19	8.33	8.20	8.30	11.35
Pr	1.57	0.03	1.57	1.57	1.66	1.59	1.20	1.19	1.20	1.59
Nd	10.87	13.66	10.71	11.08	11.26	11.06	8.44	8.47	8.49	10.10
Sm	3.39	4.17	3.39	3.57	3.58	3.51	2.8	2.74	2.76	3.51
Eu	1.27	1.48	1.24	1.30	1.31	0.28	1.09	1.09	1.10	1.29
Gd	4.94	5.90	4.86	5.21	5.35	5.23	4.21	4.08	4.20	5.26
Tb	0.91	1.08	0.9	0.96	0.98	0.96	0.78	0.77	0.77	0.95
Dy	5.30	6.21	5.27	5.66	5.75	5.60	4.51	4.46	4.47	5.56
Ho	1.14	1.33	1.11	1.22	1.24	1.20	0.99	0.99	0.98	1.20
Er	3.57	4.18	3.55	3.81	3.88	3.88	3.10	3.08	3.03	3.81
Tm	0.62	0.71	0.61	0.67	0.66	0.67	0.54	0.51	0.53	0.65
Yb	3.31	3.87	3.26	3.53	3.58	3.55	2.86	2.83	2.83	3.50
Lu	0.48	0.57	0.48	0.51	0.54	0.52	0.42	0.42	0.41	0.51
Hf	2.50	3.09	2.46	2.59	2.66	2.64	1.96	1.93	1.97	2.53
Th	0.19	0.26	0.19	0.22	0.26	0.24	0.18	0.19	0.18	0.27
U	0.10	0.09	0.11	0.12	0.10	0.08	0.15	0.09	0.06	0.13

Mg#= mol Mg/ mol (Mg+mol Fe^{2+})

Table 1 contd.

Sample no.	dr-1k	dr-1l	dr-1m	dr-2a	dr-2b	dr-2c	dr-2d	dr-2e	dr-2f
SiO_2(wt%)	51.05	51.12	51.23	51.01	50.54	50.95	50.91	51.51	50.85
TiO_2	1.48	1.5	1.51	1.5	1.33	1.26	1.8	1.36	1.25
Al_2O_3	15.6	15.51	15.44	15.56	16.23	16.36	14.94	16.28	16.6
Fe_2O_3	9.98	10	10.07	10.02	9.47	9.25	11.14	9.49	9.04
MnO	0.18	0.18	0.18	0.18	0.17	0.17	0.19	0.18	0.2
MgO	8.01	8.16	8.1	7.96	7.62	7.83	7.76	7.87	7.57
CaO	11.58	11.55	11.49	11.6	11.73	11.9	10.86	11.84	11.93
Na_2O	2.41	2.48	2.48	2.52	2.32	2.43	2.52	2.47	2.47
K_2O	0.13	0.14	0.12	0.15	0.11	0.11	0.17	0.12	0.15
P_2O_5	0.14	0.14	0.14	0.15	0.12	0.12	0.16	0.13	0.13
Total	100.56	100.78	100.76	100.65	99.64	100.38	100.45	101.25	100.19
Mg#	0.61	0.62	0.61	0.61	0.61	0.63	0.58	0.62	0.62
Sc (ppm)	36.95	36.33	36.54	38.12	34.61	36.26	33.80	38.04	36.90
V	292.70	294.22	293.59	269.07	263.96	256.64	259.36	266.84	288.94
Cr	303.57	301.35	310	347.94	302.69	314.70	282.53	329.28	275.97
Co	44.10	44.36	44.15	44.74	41.22	42.68	39.86	46.22	45.07
Ni	113.73	115.68	116.14	84.51	103.94	83.66	98.28	92.98	94.92
Cu	88.4	75.27	80.61	96.33	79.27	78.56	74.13	92.46	72.04
Zn	114.39	111.24	116.32	108.61	104.63	100.52	109.53	102.71	107.85
Ga	16.34	16.57	16.55	15.90	15.97	15.37	15.66	16.22	16.39
Rb	0.98	0.96	0.94	0.91	1.12	1.64	0.9	2.56	1.41
Sr	105.95	109.31	108.80	118.01	116.11	112.37	112.03	124.82	122.45
Y	36.64	36.20	36.32	31.01	32.10	31.76	32.20	31.15	34.85
Zr	107.41	106.33	106.39	87.20	93.79	93.92	95.88	87.99	105.98
Nb	3.36	3.22	3.30	2.39	2.65	2.63	2.80	2.56	2.50
Cs	0.02	0.02	0.02	0.02	0.04	0.09	0.02	0.16	0.03
Ba	16.73	16.99	17.82	16.85	12.62	15.48	12.95	21.02	14.07
La	3.70	3.70	3.73	3.10	3.28	3.17	3.30	3.29	3.67
Ce	11.22	11.19	11.28	9.37	10.02	9.52	10.09	9.79	11.16
Pr	1.58	1.58	1.59	1.34	1.41	1.36	1.43	1.36	1.60
Nd	10.99	10.98	10.91	9.18	9.61	9.29	9.88	9.44	10.93
Sm	3.53	3.49	3.48	2.95	3.09	2.98	3.13	2.97	3.49
Eu	1.29	1.31	1.28	1.16	1.17	1.16	1.18	1.17	1.30
Gd	5.19	5.24	5.24	4.39	4.53	4.44	4.61	4.47	5.07
Tb	0.97	0.97	0.97	0.83	0.84	0.84	0.86	0.82	0.93
Dy	5.59	5.62	5.6	4.77	4.93	4.82	4.91	4.80	5.37
Ho	1.21	1.21	1.20	1.02	1.07	1.05	1.06	1.04	1.15
Er	3.76	3.87	3.82	3.25	3.32	3.28	3.44	3.26	3.66
Tm	0.65	0.67	0.66	0.56	0.57	0.57	0.58	0.56	0.63
Yb	3.48	3.53	3.57	2.99	3.09	3.05	3.13	3.01	3.39
Lu	0.52	0.51	0.52	0.44	0.45	0.45	0.47	0.45	0.51
Hf	2.57	2.57	2.62	2.10	2.20	2.16	2.26	2.11	2.50
Th	0.36	0.26	0.27	0.20	0.20	0.27	0.18	0.27	0.24
U	0.08	0.08	0.08	0.07	0.11	0.10	0.07	0.11	0.07

Table 2

Ridge	Location (Lat/long)	Water depth (m)	Texture	Modal mineralogy (vol%)					Source
				Pl	Ol	Px	Vs	Gm	
CR	06°09′N/60°50′E	4034	Subophitic, intersertal, intergranular	34	18	3	2	43	Pluger, 1988
	03°35′N/64°05′E	3300-4100	Glassy, variolitic, intersertal, intergranular	40	5			55	Present study and Banerjee and Iyer, 1991
	01°30′S/67°39′E	3457	Quench, spherulitic, flow	21	9	tr	44	66	Pluger, 1988, Mukhopadhyay and Iyer, 1998
NCIR	05°22′S/68°15′E	2084	Intersertal, intergranular	28	16	2		64	Pluger, 1988
	5º39′S/68°03′E	3050	Intergranular, intersertal	19	2			80	Ray et al., 2009
	9º54′S/66°36′E	2000	Intergranular, intersertal	16	tr	tr		84	Ray et al., 2009
SCIR	20°30′S/66°40′E	3776	Porphyritic, quench	42	18	10	5	25	Mukhopadhyay and Iyer, 1998
	21°20′S/67°30′E	2499-3586	Spherulitic, variolitic	20	8		12	60	Pluger, 1988, Herzig and Pluger, 1988
	23°S/68°30′E	3354	Microporphyritic, variolitic	14	5		11	70	Pluger, 1988, Herzig and Pluger, 1988, Mukhopadhyay and Iyer, 1998
RTJ		n.a.	n.a	n.a.	n.a.	n.a	n.a.	n.a.	n.a

Pl: Plagioclase, Ol: Olivine, Px: Pyroxene, Gm: Groundmass, Vs: Vesicle, tr: trace, n.a.: not analyzed.

Table 3

Wt%	CR[1]			NCIR[2]			SCIR[3]			RTJ[4]		
	Max	Min	Avg	Max	Min	Avg	Max	Min	Avg	Max	Min	Avg
SiO_2	52.41	48.88	50.73 (0.61)	51.94	46.46	50.07 (1.23)	52.56	48.06	50.97 (0.88)	52.17	49.5	50.65 (0.71)
TiO_2	2.02	0.69	1.37 (0.28)	2.15	0.88	1.40 (0.29)	1.74	0.66	1.22 (0.19)	1.46	0.80	1.18 (0.22)
Al_2O_3	16.93	13.80	15.54 (0.61)	17.40	13.48	15.73 (0.82)	18.49	14.48	15.9 (0.77)	17	14.91	15.76 (0.61)
FeO_t	12.91	7.63	9.24 (0.89)	11.79	7.53	9.59 (0.96)	10.98	6.95	8.98 (0.72)	9.28	7.36	8.41 (0.72)
MgO	8.93	6.07	8.28 (0.72)	11.59	6.26	7.91 (1.09)	9.96	5.21	7.93 (0.58)	9.39	6.81	8.32 (0.66)
CaO	13.29	10.48	11.56 (0.66)	13.79	9.88	11.26 (0.72)	13.44	8.95	11.87 (0.64)	12.10	11.06	11.55 (0.37)
Na_2O	3.78	1.68	2.53 (0.37)	3.71	2.05	2.80 (0.33)	3.43	1.83	2.52 (0.27)	3.14	2.02	2.78 (0.32)
K_2O	0.29	0.04	0.13 (0.06)	0.50	0.04	0.17 (0.11)	0.68	0.04	0.14 (0.12)	0.16	0.03	0.08 (0.03)
P2O5	0.17	0.05	0.12 (0.03)	0.24	0.04	0.12 (0.05)	0.30	0.03	0.12 (0.05)	0.17	0.13	0.15 (0.02)
Total			99.68			99.22			99.81			99.06
Mg#	0.70	0.46	0.61 (0.04)	0.66	0.51	0.59 (0.05)	0.7	0.46	0.61 (0.03)	0.69	0.60	0.64 (0.03)
CaO/Al_2O_3	0.85	0.65	0.74 (0.03)	0.93	0.59	0.72 (0.06)	0.84	0.61	0.75 (0.04)	0.77	0.70	0.73 (0.02)
K_2O/Na_2O	0.11	0.02	0.05 (0.02)	0.17	0.01	0.06 (0.04)	0.24	0.02	0.05 (0.04)	0.05	0.01	0.03 (0.01)
Na_2O+K_2O	3.96	1.72	2.66 (0.41)	3.96	2.11	2.97 (0.38)	4.01	1.89	2.66 (0.35)	3.26	2.11	2.86 (0.34)

Total Fe as FeO_t and calculated as $FeO_t=0.9*Fe_2O_3t$
Mg# calculated as mol Mg/(mol Mg+ mol Fe^{2+})
Data Source:

1. Present study, Banerjee and Iyer, 1991; PetDB
2. Ray et al., 2007, PetDB
3. Murton et al., 2005; Nauret et al., 2006, PetDB
4. Price et al., 1986 ; Humler and Whitechurch, 1988 ; PetDB

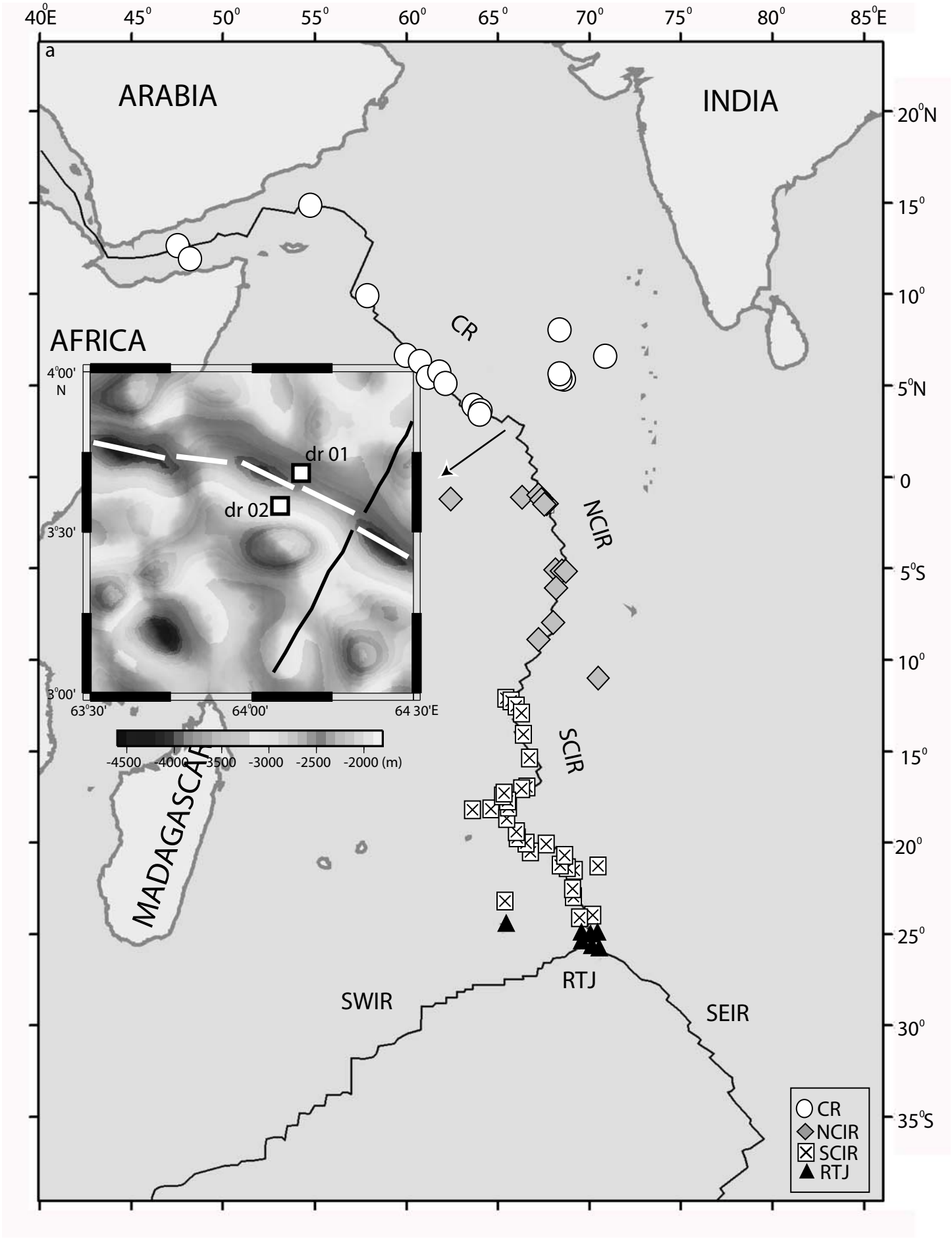
a
ARABIA
INDIA
AFRICA
MADAGASCAR
CR
NCIR
SCIR
RTJ
SWIR
SEIR
dr 01
dr 02
4°00' N
3°30'
3°00'
63°30'
64°00'
64 30'E
-4500 -4000 -3500 -3000 -2500 -2000 (m)
40°E
45°
50°
55°
60°
65°
70°
75°
80°
85°E
20°N
15°
10°
5°N
0
5°S
10°
15°
20°
25°
30°
35°S
CR
NCIR
SCIR
RTJ

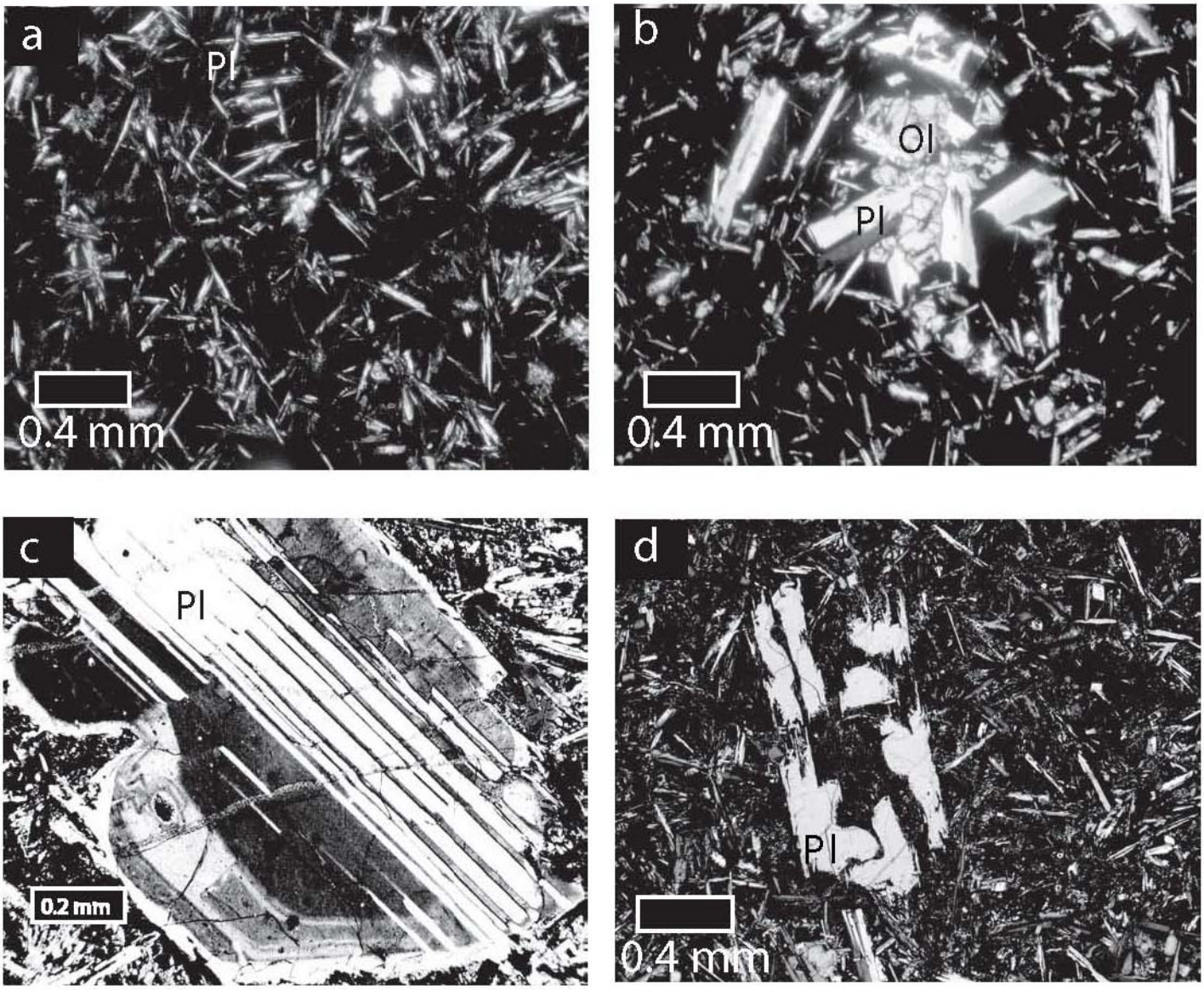
a
Pl
0.4 mm
b
Ol
Pl
0.4 mm
c
Pl
0.2 mm
d
Pl
0.4 mm

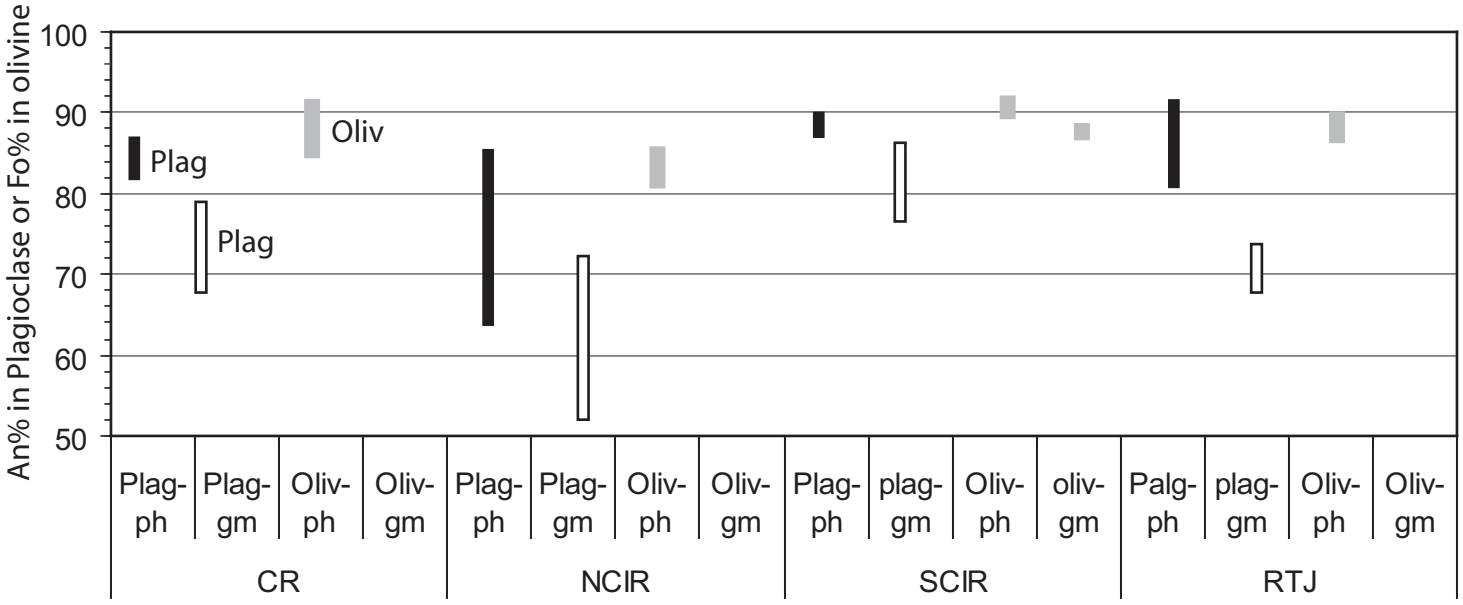
An% in Plagioclase or Fo% in olivine
100
90
80
70
60
50
Plag
Plag
Oliv
Plag-ph
Plag-gm
Oliv-ph
Oliv-gm
Plag-ph
Plag-gm
Oliv-ph
Oliv-gm
Plag-ph
plag-gm
Oliv-ph
oliv-gm
Palg-ph
plag-gm
Oliv-ph
Oliv-gm
CR
NCIR
SCIR
RTJ

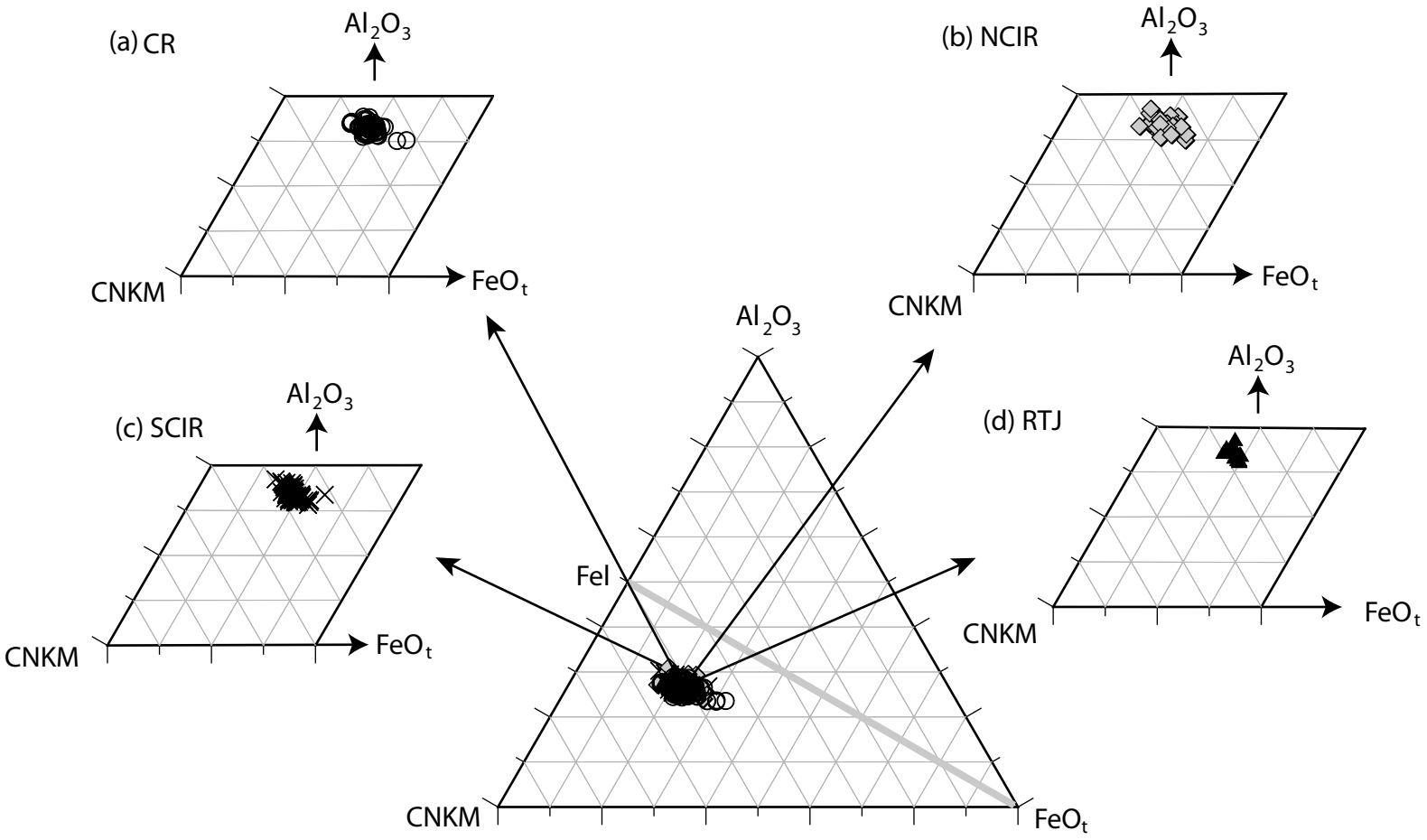
(a) CR
Al_2O_3
CNKM
FeO_t
(b) NCIR
Al_2O_3
CNKM
FeO_t
(c) SCIR
Al_2O_3
CNKM
FeO_t
Al_2O_3
FeI
CNKM
FeO_t
(d) RTJ
Al_2O_3
CNKM
FeO_t

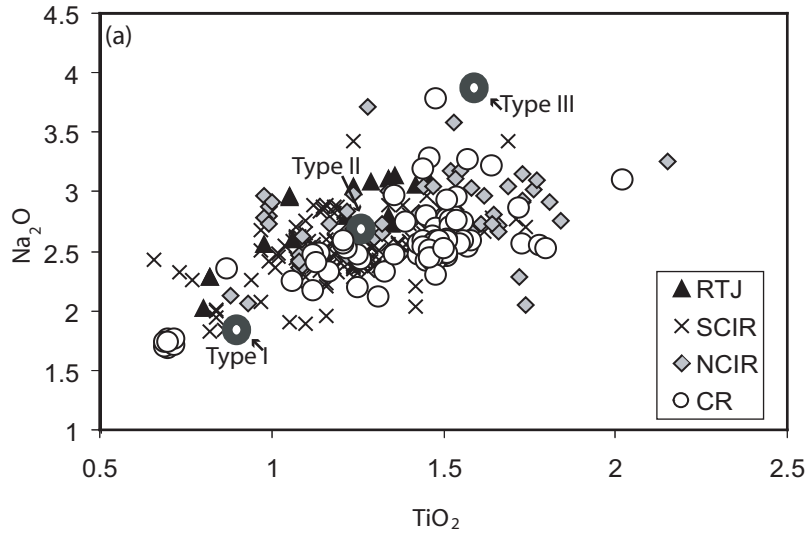
(a)
Type III
Type II
Type I
RTJ
SCIR
NCIR
CR
Na_2O
TiO_2

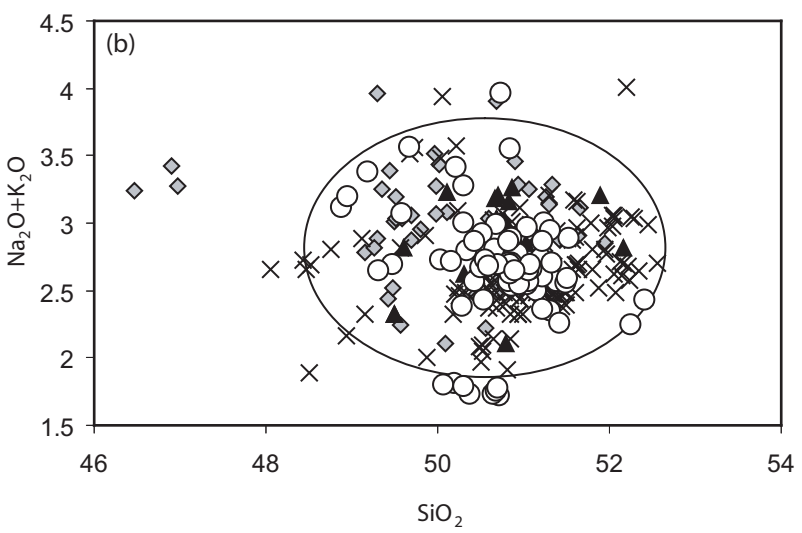
(b)
Na_2O+K_2O
SiO_2

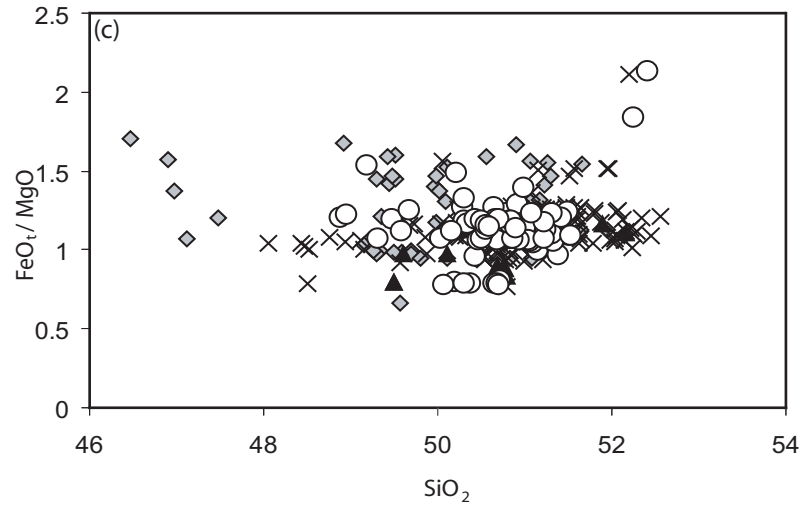
(c)
FeO_t/ MgO
SiO_2

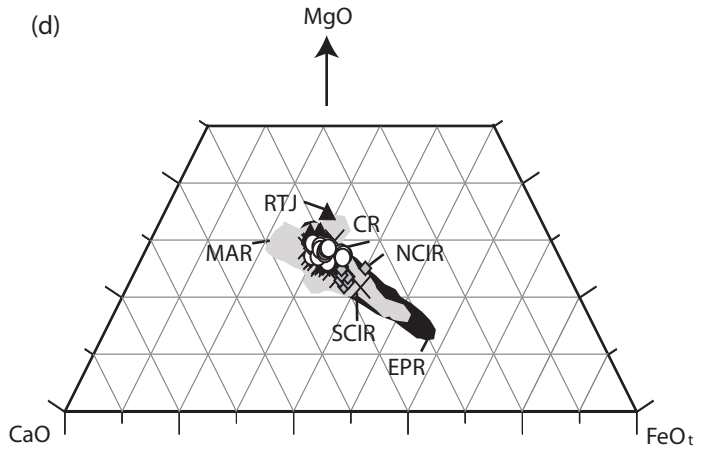
(d)
MgO
RTJ
CR
MAR
NCIR
SCIR
EPR
CaO
FeO_t

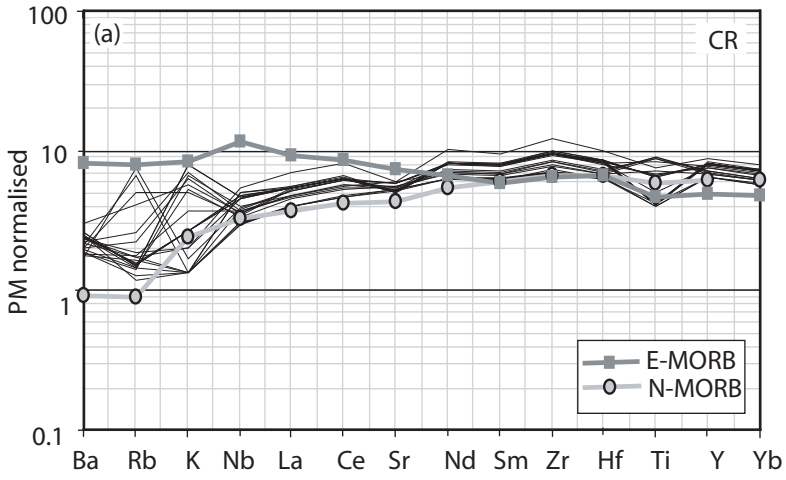
(a)
CR
100
10
1
0.1
PM normalised
E-MORB
N-MORB
Ba Rb K Nb La Ce Sr Nd Sm Zr Hf Ti Y Yb

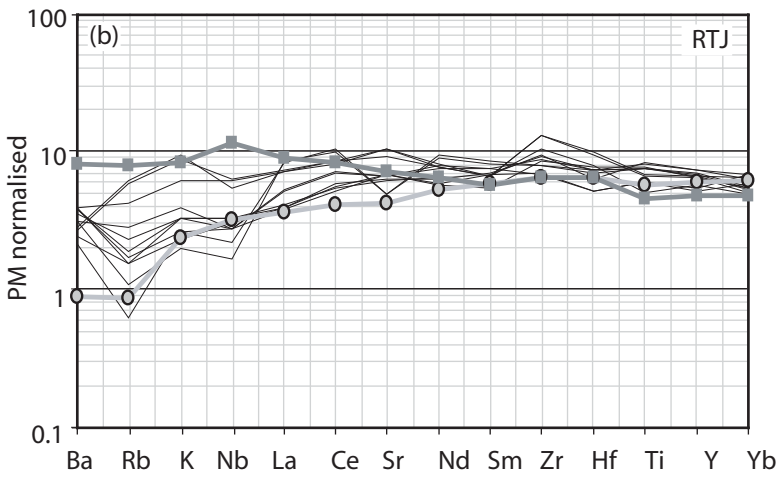
(b)
RTJ
100
10
1
0.1
PM normalised
Ba Rb K Nb La Ce Sr Nd Sm Zr Hf Ti Y Yb

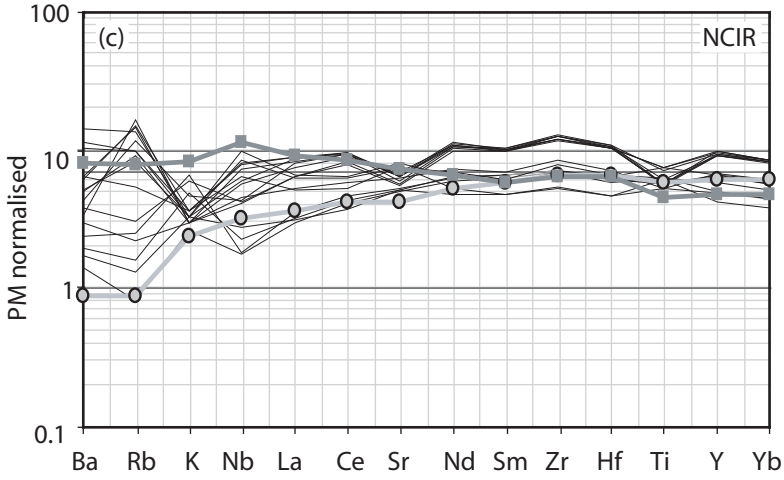
(c)
NCIR
100
10
1
0.1
PM normalised
Ba Rb K Nb La Ce Sr Nd Sm Zr Hf Ti Y Yb

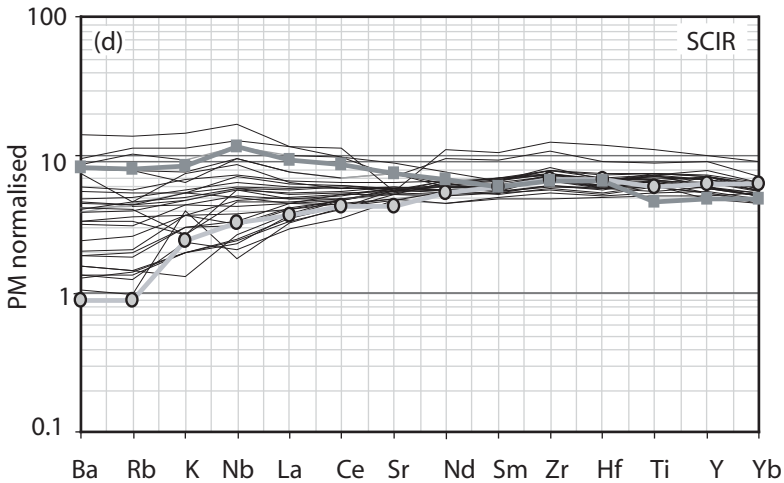
(d)
SCIR
100
10
1
0.1
PM normalised
Ba Rb K Nb La Ce Sr Nd Sm Zr Hf Ti Y Yb

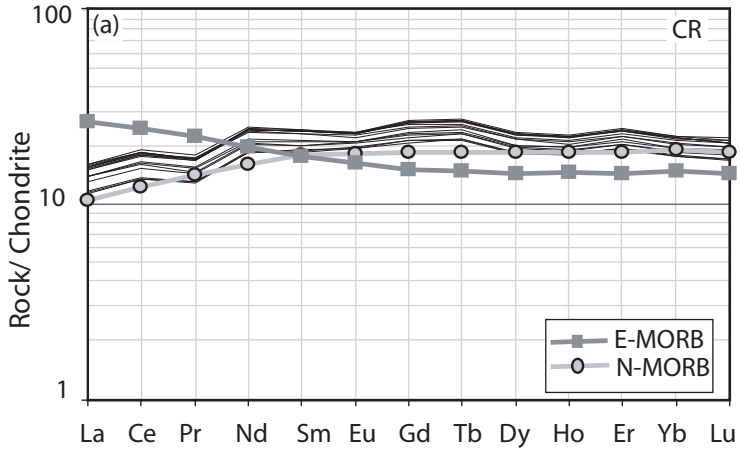
(a)
CR
100
10
1
Rock/ Chondrite
E-MORB
N-MORB
La Ce Pr Nd Sm Eu Gd Tb Dy Ho Er Yb Lu

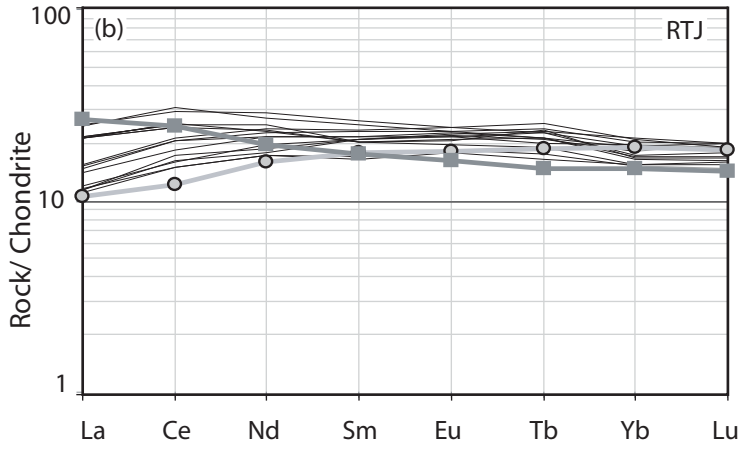
(b)
RTJ
100
10
1
Rock/ Chondrite
La Ce Nd Sm Eu Tb Yb Lu

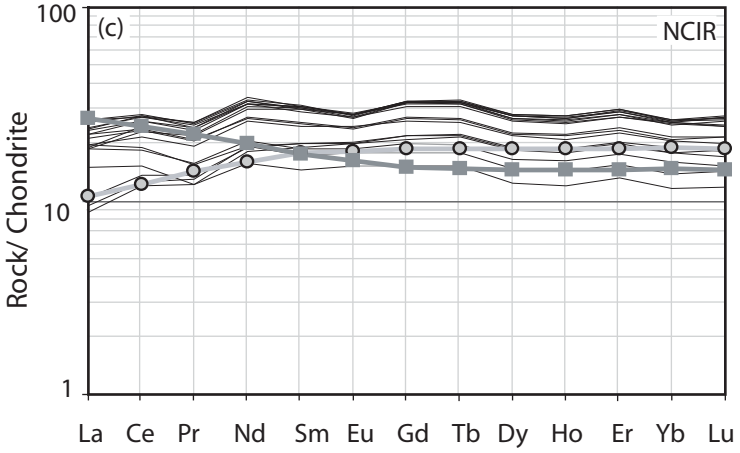
(c)
NCIR
100
10
1
Rock/ Chondrite
La Ce Pr Nd Sm Eu Gd Tb Dy Ho Er Yb Lu

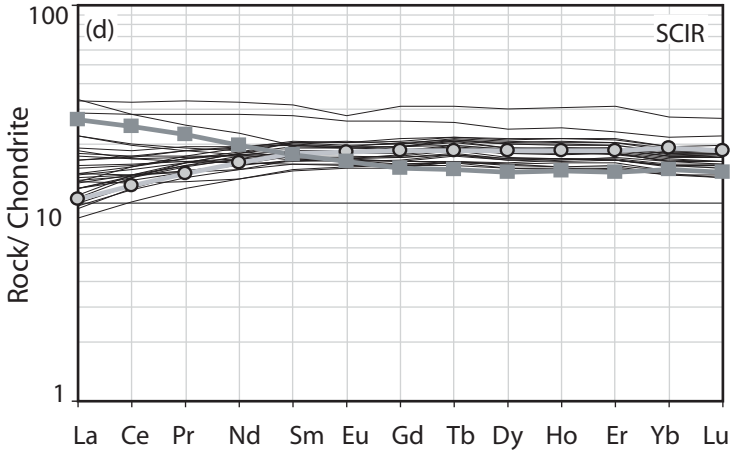
(d)
SCIR
100
10
1
Rock/ Chondrite
La Ce Pr Nd Sm Eu Gd Tb Dy Ho Er Yb Lu

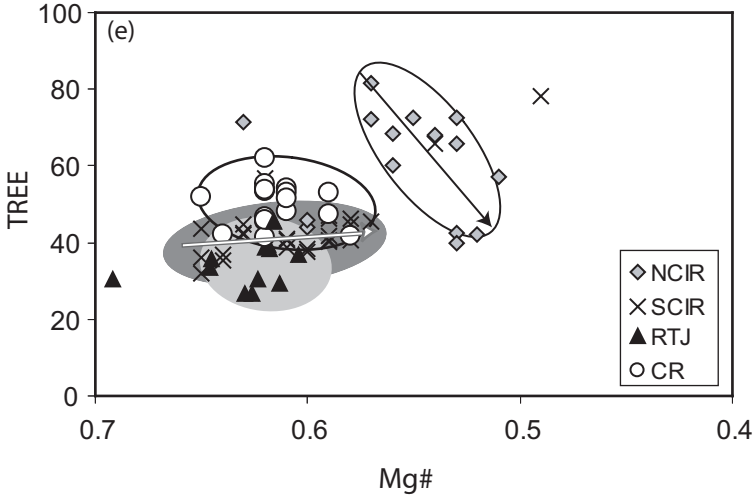
(e)
100
80
60
40
20
0
TREE
0.7
0.6
0.5
0.4
Mg#
NCIR
SCIR
RTJ
CR

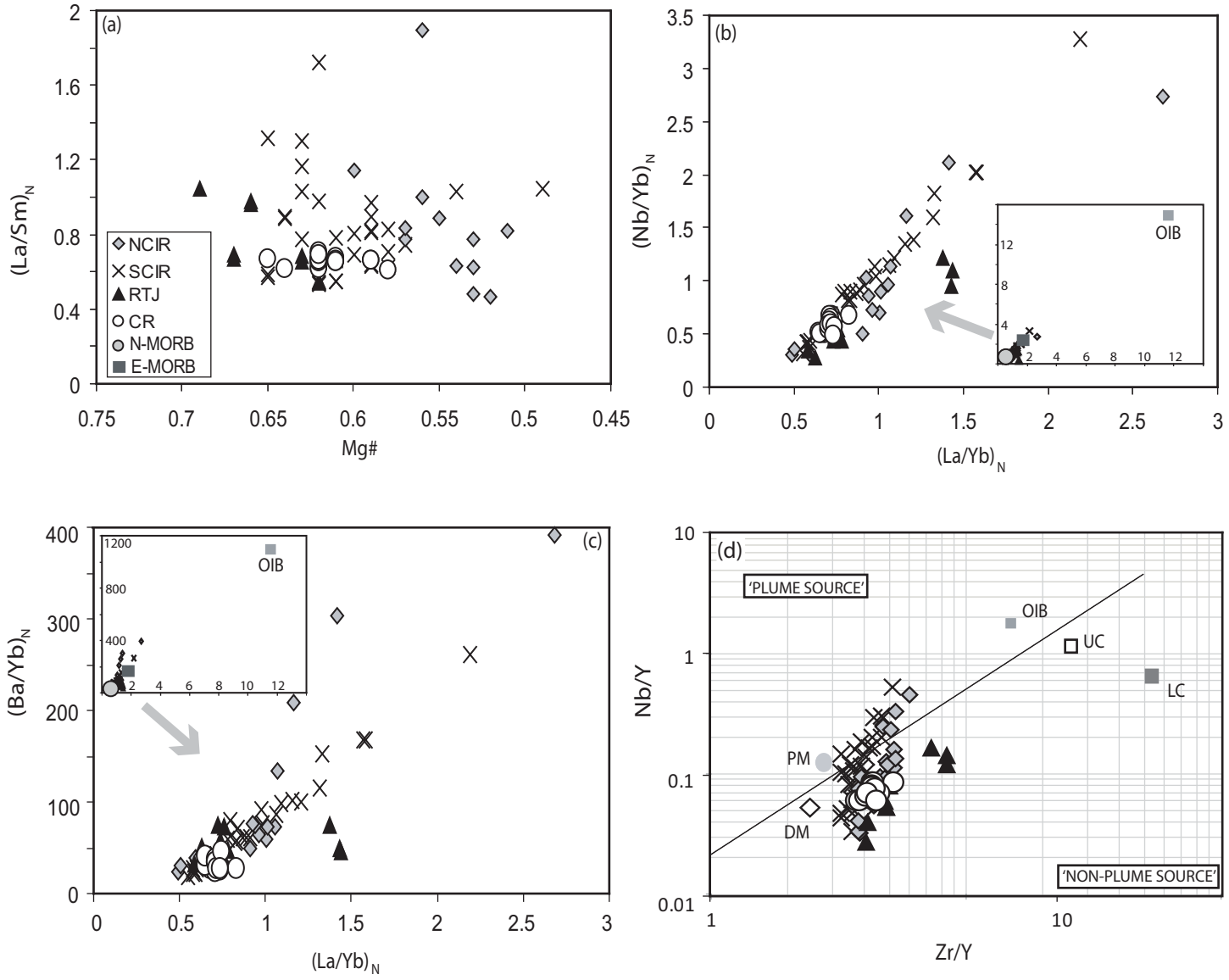
(a)
(La/Sm)N
Mg#
NCIR
SCIR
RTJ
CR
N-MORB
E-MORB
(b)
(Nb/Yb)N
(La/Yb)N
OIB
(c)
(Ba/Yb)N
(La/Yb)N
OIB
(d)
'PLUME SOURCE'
'NON-PLUME SOURCE'
Nb/Y
Zr/Y
OIB
UC
LC
PM
DM

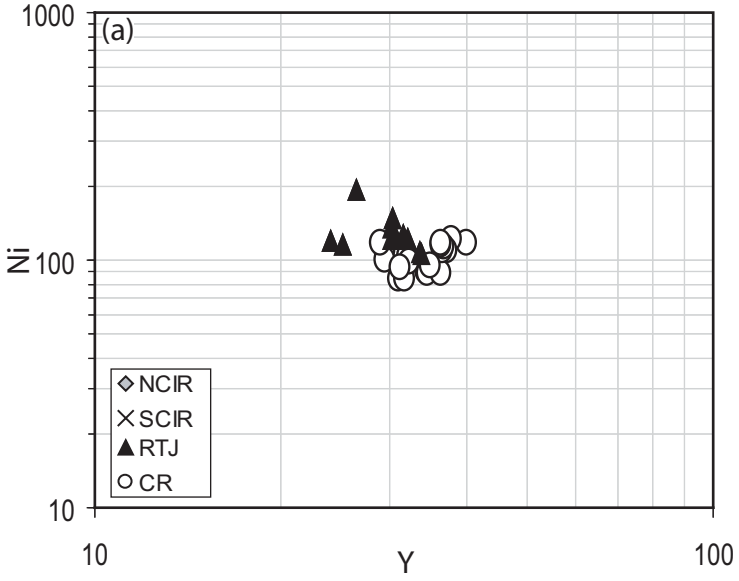
(a)
1000
100
10
Ni
10
Y
100
NCIR
SCIR
RTJ
CR

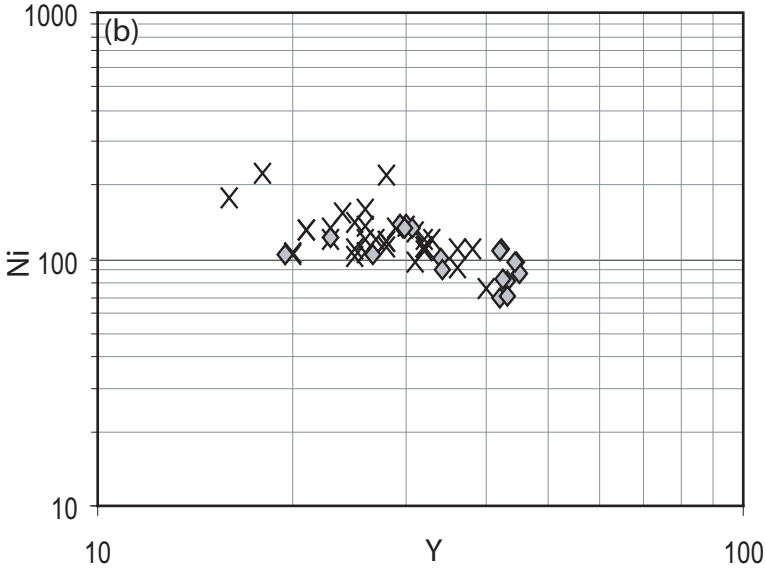
(b)
1000
100
10
Ni
10
Y
100

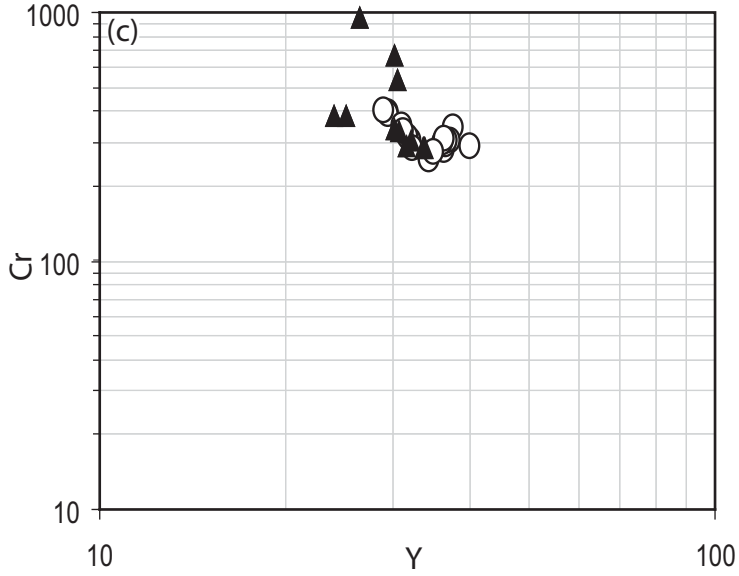
(c)
1000
100
10
Cr
10
Y
100

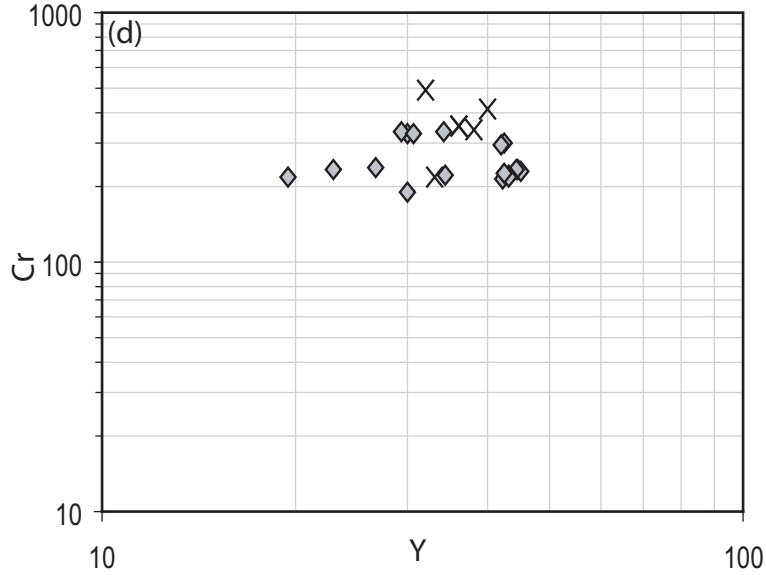
(d)
1000
100
10
Cr
10
Y
100

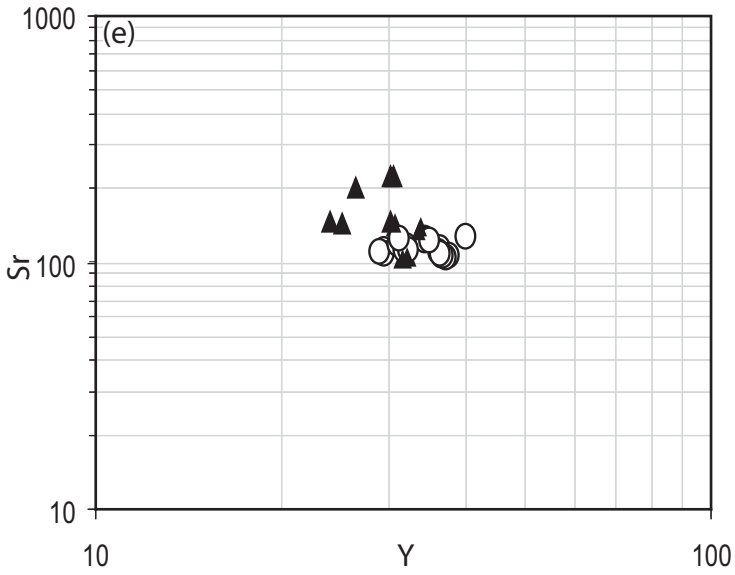
(e)
1000
100
10
Sr
10
Y
100

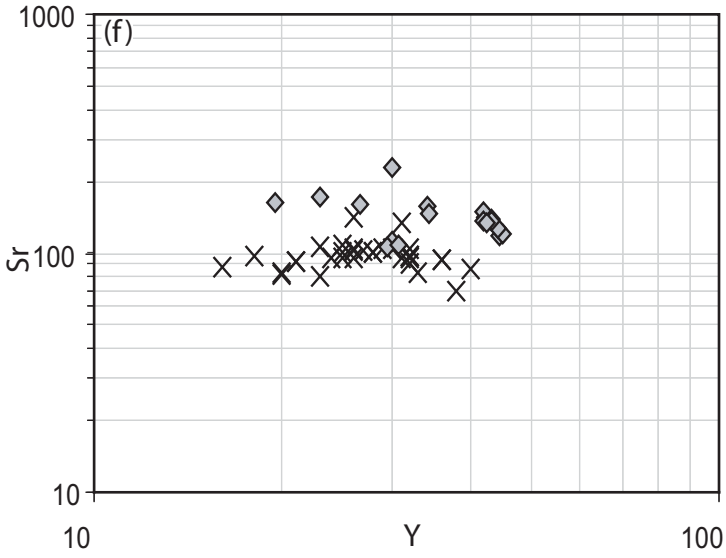
(f)
1000
100
10
Sr
10
Y
100

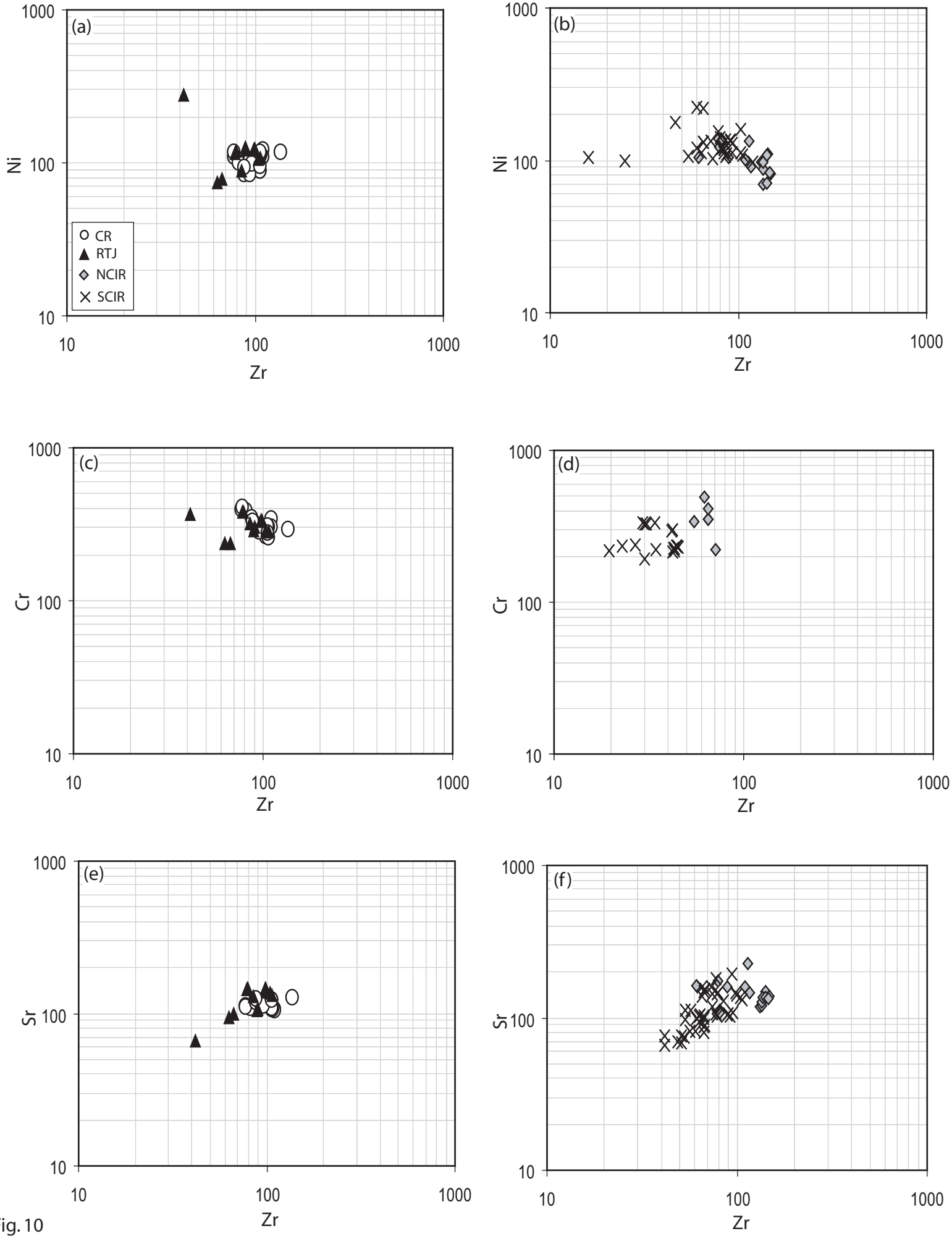

Fig. 10

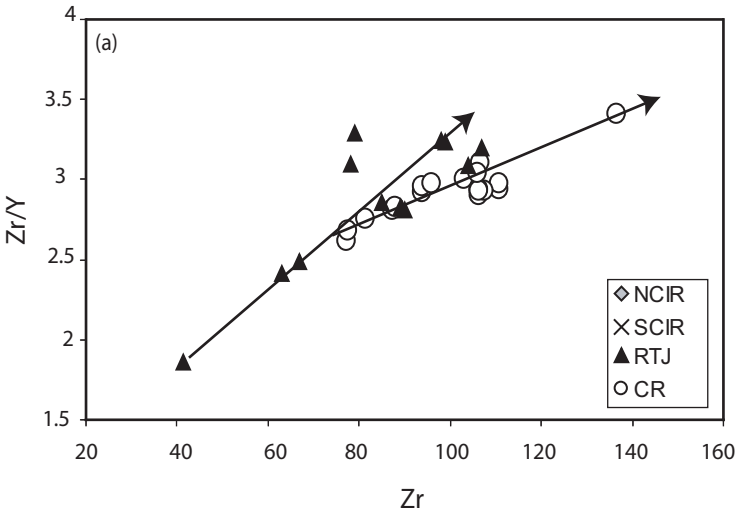
(a)
Zr/Y
Zr
NCIR
SCIR
RTJ
CR

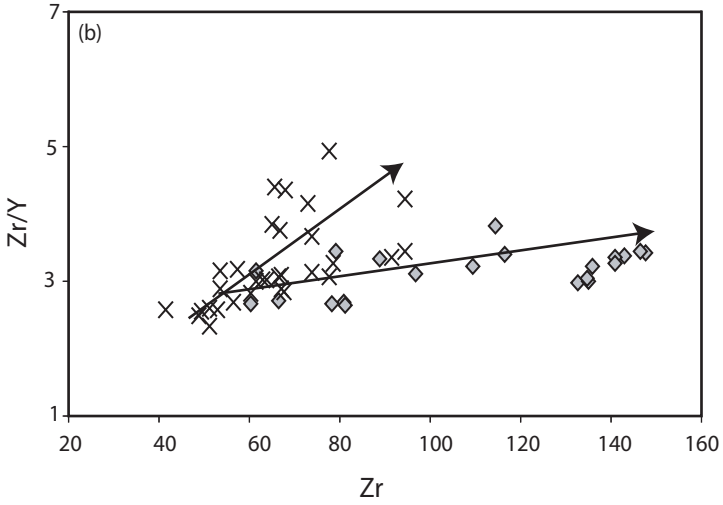
(b)
Zr/Y
Zr

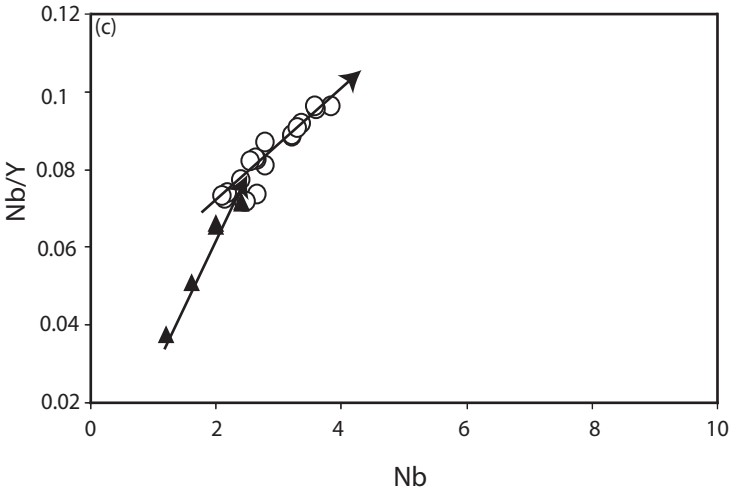
(c)
Nb/Y
Nb

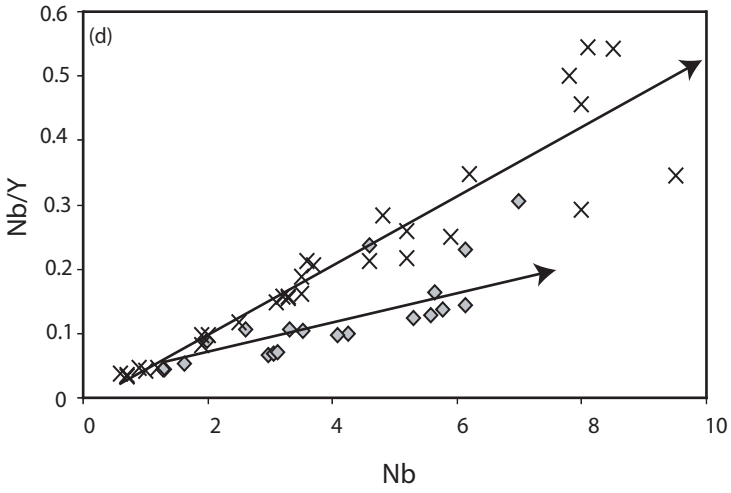
(d)
Nb/Y
Nb

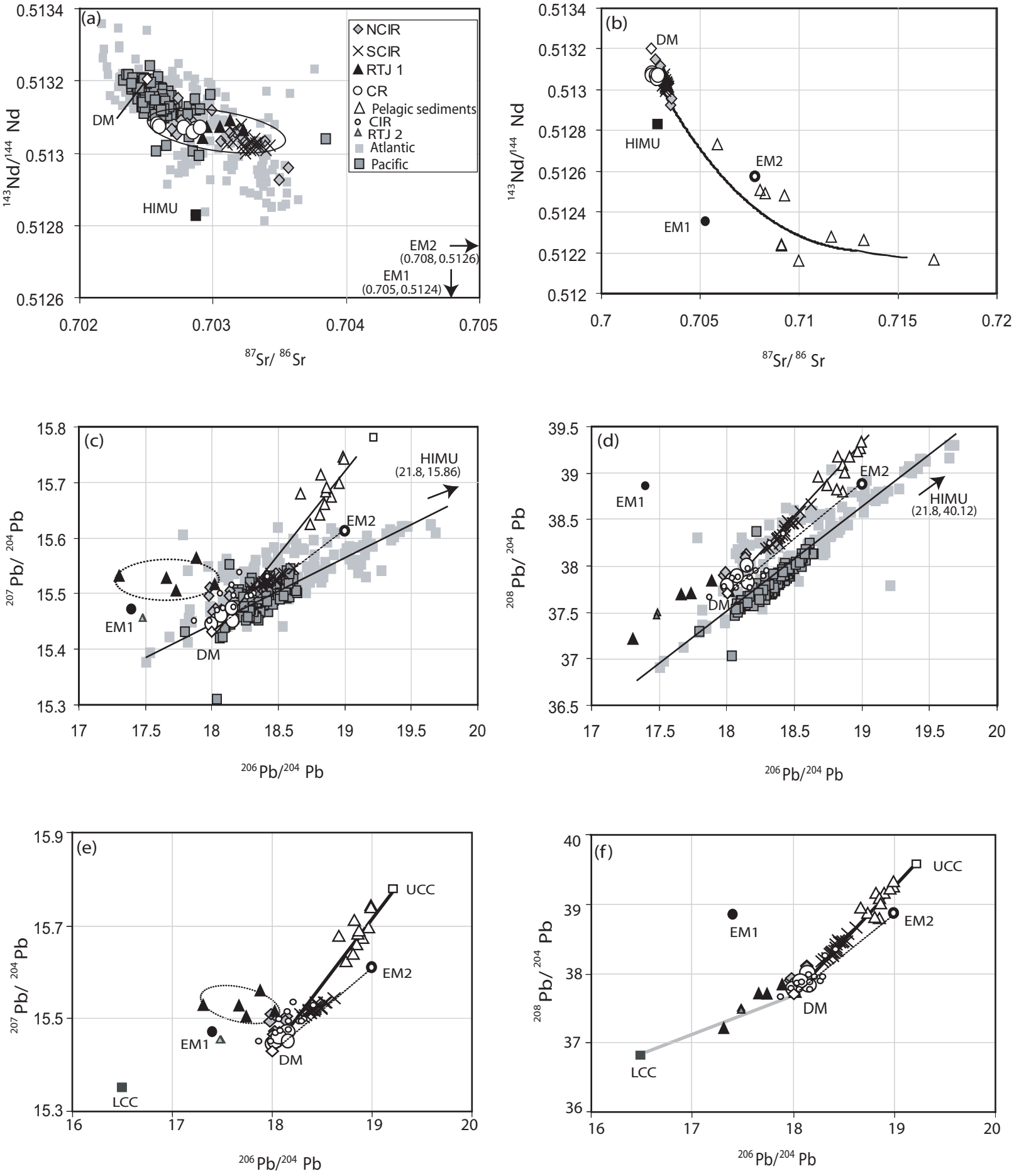
(a)
NCIR
SCIR
RTJ 1
CR
Pelagic sediments
CIR
RTJ 2
Atlantic
Pacific
DM
HIMU
EM2
(0.708, 0.5126)
EM1
(0.705, 0.5124)
143Nd/144 Nd
87Sr/ 86Sr
(b)
DM
HIMU
EM2
EM1
143Nd/144 Nd
87Sr/ 86 Sr
(c)
HIMU
(21.8, 15.86)
EM2
EM1
DM
207 Pb/ 204Pb
206Pb/204 Pb
(d)
EM1
EM2
HIMU
(21.8, 40.12)
DM
208 Pb/ 204 Pb
206Pb/204 Pb
(e)
UCC
EM2
EM1
DM
LCC
207 Pb/ 204Pb
206Pb/204 Pb
(f)
UCC
EM1
EM2
DM
LCC
208 Pb/ 204 Pb
206Pb/204 Pb